Scale Decomposition of the Water Budget in a Regional Climate Model

Soline Bielli* and René Laprise
Département des Sciences de la Terre et de l'Atmosphère, Université du Québec à Montréal

1. Introduction

The purpose of this work is to study the added value (AV) provided by a regional climate model (RCM) with respect to the global climate model (GCM) or global analyses used to drive the regional simulation. Three main factors contribute to the AV: the lateral boundary conditions (negative feedback), the discretisation (positive feedback) and finally the non-linear interactions between different scales (positive feedback). The objective is to assess the contribution of this later factor to the AV. The water plays a key role in the energetics of the climate and a better understanding of its cycle is necessary to better understand climate change. Also, precipitation produced by GCM shows large differences compared to precipitation produced by RCM as it is greatly influenced by topographic and small-scale regional features as well as regional mesoscale circulation. The water budget is thus chosen for the scale decomposition.

2. Water Budget and Methodology

The water budget is defined as: $d_t \overline{Q} = \square\square.\overline{F} + E \square P$

where $\overline{F} = \overline{UQ} = \frac{1}{g}\int_{sfc}^{top} U(x,y,p)\,\square Q(x,y,p)\,dp$

is the horizontal moisture flux, Q is the humidity, U is the horizontal wind, E the evapotranspiration and P the precipitation. To isolate the contribution of different scales, the Discrete Cosine Transform (DCT) is used as it allows efficient decomposition of non-periodic fields (see Denis *et al*. 2002 for details). The divergence of the moisture flux, which is a quadratic term, is handled as follow. The humidity Q is defined as: $Q=Q_0+Q_L+Q_S$ where Q_0 represents the very large scales that are not resolved by the RCM (as a first approximation it is defined as the domain-mean value), Q_L represents large scales that are both resolved by the RCM and the NCEP analyses (scales greater than 600 km) and Q_S represents the small scales that are only resolved by the RCM (scales smaller than 600 km), which represents the AV of the RCM. The same decomposition is applied to both components of the horizontal wind U. The vertically integrated moisture flux is then written as:

$$\overline{F} = \overline{F}_0 + \overline{F}_G + \overline{F}_S \text{ and}$$

$$\overline{F} = \sum_{k\,\square\,(0,G,P)} \sum_{l\,\square\,(0,G,P)} \overline{U_k Q_l} = \overline{U_0Q_0} + \overline{U_0Q_L} + \overline{U_0Q_S} + \overline{U_LQ_0} + \overline{U_LQ_L} + \overline{U_LQ_S} + \overline{U_SQ_0} + \overline{U_SQ_L} + \overline{U_SQ_S}$$

Finally the divergence of each of the 9 terms is calculated. One must keep in mind that each term can contribute to any of the 3 defined scales as they represent non-linear interactions.

3. The Canadian Regional Climate Model and its driving data

The Canadian regional Climate Model (CRCM) described in Caya and Laprise (1999) is used for a simulation with 45-km horizontal resolution and 29 sigma levels, and driven by NCEP reanalyses. A winter month simulation (Feb. 1990) is used over a domain of about 6000 km by 6000 km centred over Canada. The simulation outputs are interpolated on the 17 pressure levels of the NCEP reanalyses. The NCEP analyses have a T32 resolution and are interpolated over the CRCM 45-km horizontal grid. A mask (Boer 1982) is used to remove the values that are below the ground level using the CRCM surface pressure.

* *Corresponding author address*: Soline Bielli, Université du Québec à Montréal, Ouranos, 550 rue Sherbrooke Ouest, 19e, Montréal, QC, H3A 1B9, Canada. E-mail: bielli@sca.uqam.ca

4. Divergence of the moisture flux and its decomposition

The divergence of the moisture flux for 15 Feb. 1990 is displayed on Fig. 1 where one can see two main structures: a dipole of convergence-divergence over the east coast of America associated with a north-south band of precipitation often observed during winter time, a second dipole over the ocean with a west-east orientation. Fig. 2 displays the 9 decomposed terms of the divergence flux. It shows that large-scale dominant terms are those involving the large-scale humidity (U_0Q_L and U_LQ_L). The dominant small-scale terms are those related to the small-scale humidity with large and very large scale winds (U_0Q_S and U_LQ_S). These last two terms tend to modulate the large-scale structures that are represented in the large-scale terms such as to increase the central amplitude of the features and to decrease their spatial extension. The term involving only small scales U_SQ_S is weaker but shows also an interesting signal. The same decomposition is applied to the NCEP driving data (not shown) and results show that the cross-

term that involved small-scale terms have no contribution, as expected. Indeed, the added value of the RCM is dominantly represented by non-linear interactions between small- and large- scale features in this case. The large-scale structure of the divergence is very close to the pattern seen on the CRCM decomposition.

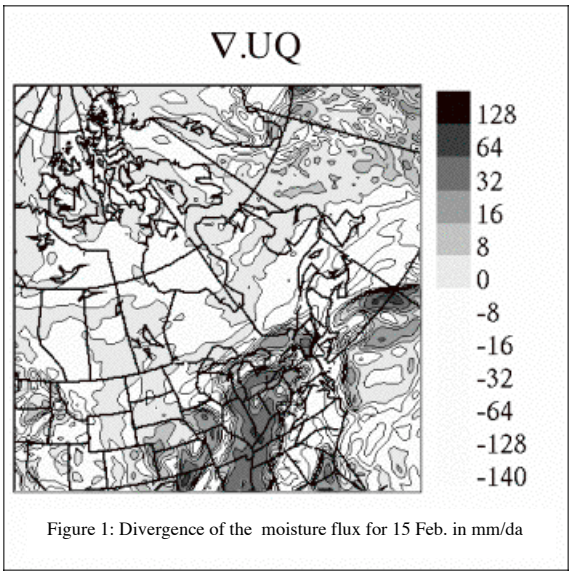

Figure 1: Divergence of the moisture flux for 15 Feb. in mm/da

References

Boer, G. J. 1982: Diagnostic equations in isobaric coordinates. *Mon. Wea. Rev.*, 110, 1801-1820

Caya D and R. Laprise 1999: A semi-implicit semi-Lagrangian regional climate model: The Canadian RCM. *Mon. Wea. Rev.* 127, 341-362

Denis, B., J. Côté and R. Laprise, 2002: Spectral decomposition of two-dimensional atmospheric fields on limited-area domains using the discrete cosine transform (DCT). *Mon. Wea. Rev.*, 130, 1812-1829

Figure 2: The 9 terms of the scale decomposition of divergence of the moisture flux for 15 Feb. 1990 in mm/da for the CRCM simulation. The U_SQ_S term is displayed with a different colour scale than the other terms.

Effect of Surface Heating over Indochina on the Summer Monsoon over South China

K. C. CHOW* AND JOHNNY C. L. CHAN
Laboratory for Atmospheric Research, Department of Physics & Materials Science
City University of Hong Kong, Hong Kong, China
*E-mail: apkchow@cityu.edu.hk

1. Introduction

The onset of the Asian summer monsoon is commonly considered to begin firstly over the region of the Bay of Bengal and Indochina. From climatology, a heating center can be found over the Indochina Peninsula in May when this first transition of summer monsoon occurs. This heating center is characterized by the presence of an anticyclone in the upper troposphere. While it appears that the development of the heating center over the Indochina region is important to the onset of the Southeast Asia monsoon, the factors that determine its establishment and location are not clearly known. Since the heat capacity of land is generally much less than that of the ocean, solar radiation reaching land surfaces can go back to the atmosphere quickly. Considering this point and the particular geographical location of Indochina, this study aims to examine the heating effect of the Indochina landmass in the development of the heating center and the onset of the summer monsoon over south China.

2. Model and experiment design

The model used in this study is a regional climate model developed by the China National Climate Center and the City University of Hong Kong, based on the NCAR RegCM2. The design of the experiments for the present study is to isolate the thermal effect of the Indochina landmass on the atmosphere, so that when comparing with the results of the control run (CTRL), the heating effect of the Indochina landmass can be estimated.

Two sensitivity experiments have been carried out for the year 1998. In the first experiment, the longwave radiation emission from the ground is set to be equal to that reaching the ground. For heat exchange at the surface, the surface sensible heating and evaporation are turned off. With such a setting, the presence of the Indochina landmass should have no particular effect on the atmosphere other than providing the drag. In another experiment (EXPIC_HT), the same setting on the longwave radiation and sensible heat flux is applied, but surface evaporative flux is allowed. The objective of the second experiment is to investigate the contribution of the surface heating (long wave radiation + sensible heating) over the Indochina landmass in the total heating effect.

3. Results

Results of the two experiments show that over Indochina, surface heating is much more significant on both the monsoon circulation and precipitation, compared with the effect of surface evaporation or latent heat. Some preliminary results of EXPIC_HT are as follows. The effect of surface heating of the Indochina landmass on the Asian summer monsoon is most significant in May while its effect is much less in June. Precipitation is reduced significantly in southern China and the western North Pacific (Fig. 1). In the lower troposphere, the heating effect induces an anomalous negative height field so that an anomalous cyclonic circulation occurs over eastern China and the western North Pacific (Fig. 2a). The result is a reduction in the strength of the southwest monsoon. The anomalous geopotential height fields show a northeastward shift as the monsoon season proceeds. The anomalous flow and geopotentail height fields in the upper troposphere are closely related to those in the lower troposphere but with reverse phases (Fig. 2b). However, the amplitudes of the anomalies are much larger than those in the lower troposphere. This indicates the sign of upper atmospheric heating and suggests that the corresponding atmospheric circulation in the lower troposphere may be driven by this heat source.

Acknowledgments. This research is sponsored by the Research Grants Council of the Hong Kong Special Administrative Region of China Grant CityU 2/00C.

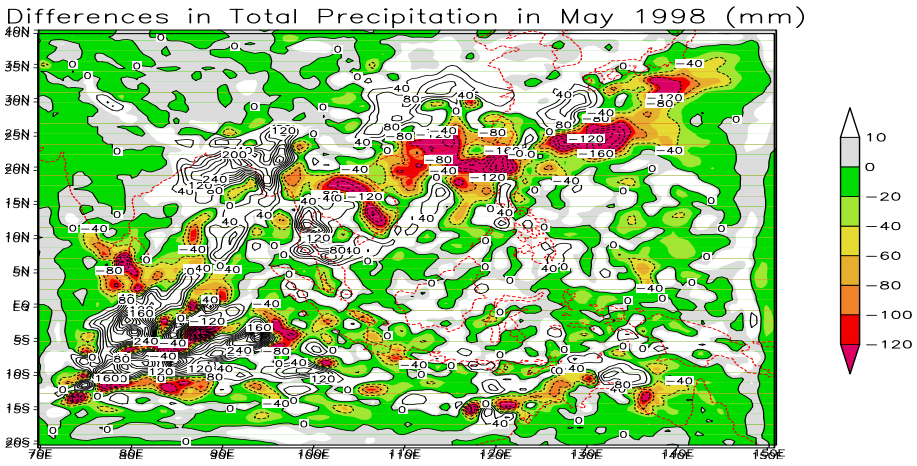

Fig. 1. Differences in precipitation (EXPIC_HT – CTRL) for May 1998. Unit: mm.

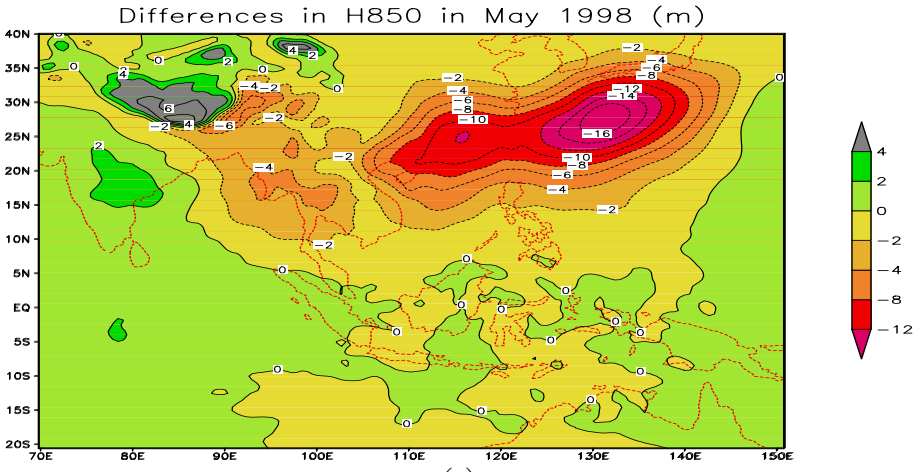

(a)

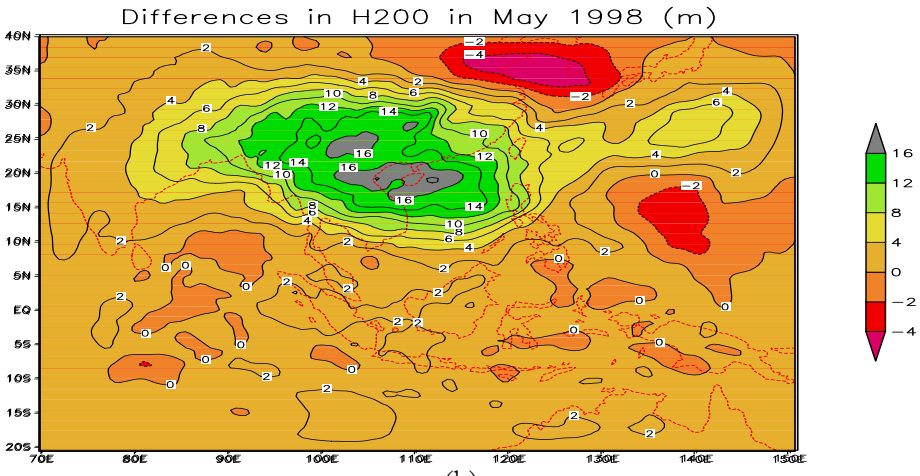

(b)

Fig. 2. As in Fig. 1 except for geopotential heights at (a) 850 hPa (b) 200 hPa. Unit: gpm.

Mediterranean convection and climate change

Michel Déqué, Florence Sevault and Samuel Somot
Météo-France/CNRM 42 av. Coriolis 31057, Toulouse, France

There are a few places in the world ocean where surface water sinks due to buoyancy loss and contributes to the global thermohaline circulation. They are located in the polar regions and the recycling time scale is millennial. This phenomenon is named oceanic convection, as it is the symmetrical phenomenon of atmospheric convection. The Mediterranean Sea is also a place where surface Atlantic water entering through the Gibraltar Strait is transformed into deep water and sent back one century later to the Atlantic with modified characteristics. According to IPCC projections, the Mediterranean basin would become warmer and drier by the end of the 21st century. A radiative warming would stabilize the surface layers and reduce convection (water density decreases with temperature), whereas an increase of the fresh water deficit would increase convection (a higher salinity implies a higher density). An important question is the resulting effect of these two competing phenomena. Indeed, convection plays a major role in the Mediterranean Sea ecosystems.

A 140-year numerical simulation has been conducted with a climate version of the ARPEGE/IFS atmospheric model. This global model has a maximum resolution of 0.5° in the Mediterranean basin (Gibelin and Déqué, 2003). The simulation covers the 1961-2100 period. Up to 2000, sea surface temperature (SST) as well as greenhouse gas and aerosol concentration are imposed from observed values. Then, an IPCC-A2 scenario is prescribed. SST is calculated by adding to observed monthly values an anomaly evaluated through a former ARPEGE simulation coupled to a global ocean and sea-ice model (OPA/GELATO). The horizontal resolution of the coupled model is 2.8° for the atmosphere, a little higher for the ocean. The numerical drift (estimated through a control experiment), and the systematic error of the SST are removed. This regional simulation is part of the Météo-France contribution to the European PRUDENCE project.

Daily fluxes of momentum, heat, and water over the Mediterranean Sea from the above-mentioned simulation have been used as a forcing for a regional ocean model OPAMED8 covering the whole Mediterranean Sea with a resolution of about 10 km. This model has a buffer zone in the near Atlantic in which a relaxation of temperature and salinity is applied. The relaxation fields come from the above-mentioned coupled global scenario with ARPEGE in low resolution. River run-off (including the fresh water inflow at the Dardannelles Strait) is calculated from a routing scheme (TRIP) using the grid-point run-off of the variable resolution scenario with ARPEGE. Thus, in comparison with earlier studies, no relaxation is imposed in the Mediterranean Sea, except the unavoidable adaptation of surface heat flux to SST. In particular there is no constraint on salinity other than the A2 scenario.

The time scales of an ocean model are much longer than those of an atmosphere model. As there is no relaxation, a numerical drift could occur in the simulation and could be misinterpreted as a climate signal. For this reason, a control oceanic simulation has been performed, in which the fluxes of the 1981-2100 period are those of the 1961-1980 period (with a 20-year loop).

Our results clearly show that the thermal effect dominates the salinity effect, and that the convection intensity decreases significantly. Figure 1 shows the mixed layer depth in winter and in the western basin south of the French coast (a place and a season with maximum convection). The pattern is stable after 100 years in the control simulation, but the mixing vanishes in the scenario.

In this study the feedback of regional scale SST anomalies on the atmosphere is neglected. This is also the case of the feedback from the Atlantic Ocean, but the time scale is much larger than a century. The next step in this study of possible evolution of the Mediterranean oceanic circulation during the 21st century is to couple OPAMED8 with ARPEGE. This has been done with a 30-year control simulation, but the coupled system needs to be improved before attempting centennial simulations.

This study has been partly supported by the European Commission through the PRUDENCE project (EVK2-CT-2001-00132) and by the French Environment Department through the GICC-MedWater project.

Gibelin, A.L., and Déqué, M., 2003: Anthropogenic climate change over the Mediterranean region simulated by a global variable resolution model. Clim. Dyn., 20,327-339.

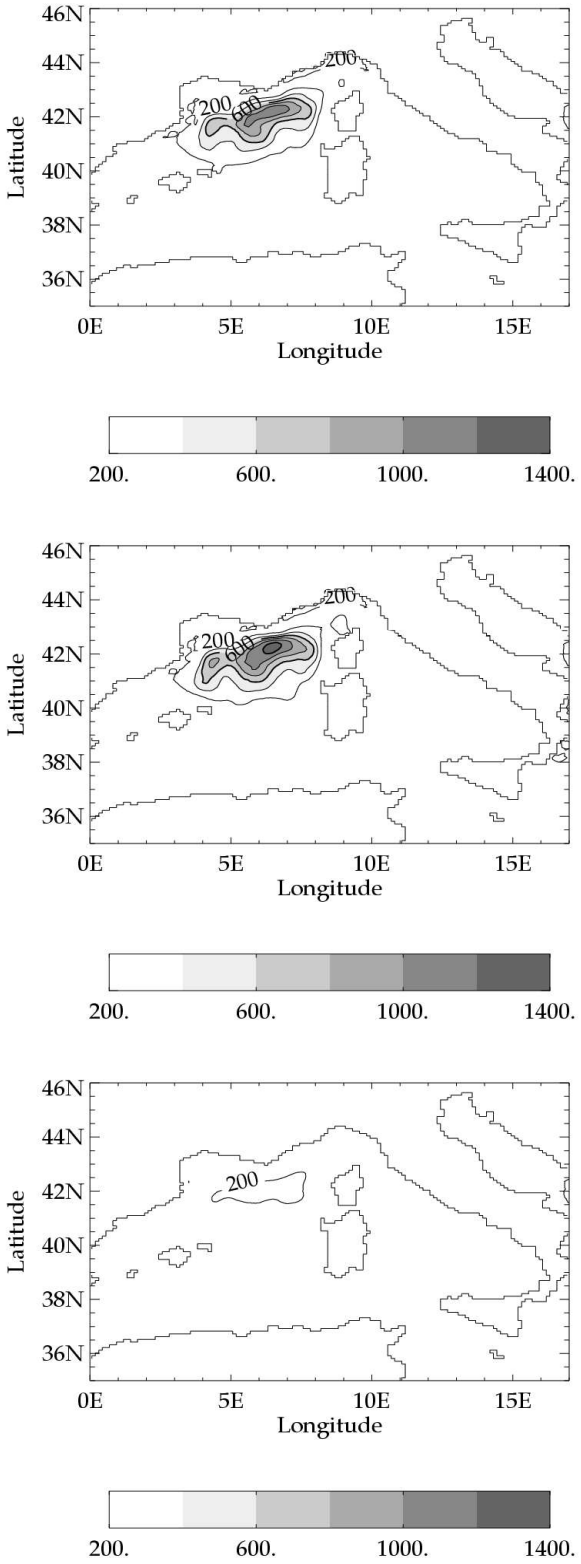

Figure 1: Winter (JFM) mixed layer depth (m) in the western Mediterranean basin convection area: beginning of the control run 1961-2000 (top), end of the control run 2071-2100 (middle) and end of the IPCC-A2 scenario 2071-2100 (bottom).

Baltic Sea Climate Scenarios for Sea Surface Temperature and Ice.

Ralf Döscher and H.E.Markus Meier, Rossby Centre at SMHI, Norrköping/Sweden

A mini-ensemble approach is taken to quantify possible changes in Sea Surface Temperature (SST) and sea ice extent of the Baltic Sea in response to atmospheric greenhouse scenarios. Mean quantities, interannual variability and uncertainty are addressed.

The Rossby Centre regional coupled ocean-ice-atmosphere model RCAO (Döscher et al. 2002) in a northern European domain is applied to dynamically downscale global control and scenario simulations from two global models (HadAM3H ("HC") and ECHAM4/OPYC3 ("MPI")) and two emission scenarios (A2 and B2, see Nakicenovic et al. 2000). RCAO has been run for today's climate (1961 - 1990, 'control run') and for future time slices (2071-2100, 'scenario run'). Details on the component models of RCAO can be found in Jones et al. (2004) for the atmosphere (RCA) and in Meier et al. (2003) for the ocean and ice model (RCO).

Some conclusions on robustness and ambiguity of projected climate change are possible only due to the availability of several control and scenario experiments (2+4). This represents major progress compared to earlier regional investigations. The regional simulation length allows for statistical significance in the change of not only mean SST but also of the mean annual cycle of heat flux. Furthermore, frequency distributions and interannual variability of monthly mean SST would not be meaningful with shorter experiments. Another general improvement of regional scenario technique is seen in the consistent model set up. The ocean model interacts directly with the atmosphere model, rather than passively accepting forcing in offline standalone runs, which might be affected by the imprint of a simpler representation of the sea surface. Detailed results can be found in Döscher and Meier (2004) for temperature and heat fluxes and in Meier et al. (2004) for sea ice and impact on the Baltic's seal habitat.

	mean SST in ^{o}C	SST change scenario-control in ^{o}C	Mean max annual ice volume in 10^9 m^3	Change of mean max annual ice volume (scenario – control) in 10^9 m^3	Change of mean max annual ice volume (scenario – control) in %
Observations	7.2	-	-		
HCCTL	7.7	-	42.4		
MPICTL	7.3	-	46.9		
HCA2	10.7	+ 3.0	7.1	-35.3	-83
MPIA2	11.1	+ 3.8	4.1	-42.1	-90
HCB2	9.6	+ 1.9	10.2	-32.2	-76
MPIB2	10.2	+ 2.9	8.2	-38.7	-83
average change	-	+ 2.9		-37.1	-83

Table 1. 29-year mean SST and sea ice volume. The SST observations are climatological monthly means calculated by Janssen et al. (1999) . Model runs are denoted as combination of the name of the driving GCM (HC, MPI) and the type of run (CTL for control or A2/B2 for the scenario runs).

The Baltic Sea mean SST for the different runs are given in table 1 together with climatological observations. SST mean values of the control simulations show only small positive biases of less than 0.6 ^{0}C. These differences correspond to a generally too warm surface air temperature over Europe in the regional atmosphere model (Räisänen et al., 2003). The ensemble mean surface warming is 2.9 ^{0}C. The uncertainties due to the emission scenario and the global model are indicated by the differences between the individual experiment's signals. Warming is stronger for the A2 cases (3.4 ^{0}C on average) and smaller for the B2 cases (2.4 ^{0}C on average). Surface warming based on MPI scenarios is stronger than HC-based increases by 0.9 ^{0}C. Differences are consistent with the greenhouse gas scenarios and the associated global mean GCM and regional mean RCM surface air temperature (Räisänen et al., 2003). Sea surface warming is strongest during the period May to September for all cases.

Interannual variability of Baltic Sea SST is increased by up to 0.5 ^{o}C in terms of standard deviation of individual monthly means. The related frequency distribution for SST (i.e. the distribution of colder and warmer than normal years) is smoothed in northern basins during the colder period of the year as not limited by the freezing point temperature.

The Baltic Sea heat budget has been calculated for control and scenario experiments. Both show similar total surface heat fluxes close to zero. Component fluxes show robust and coherent changes under a warmer climate: solar radiation is increased, net longwave radiation (out of the ocean) is increased, sensible heat flux (out of the ocean) is reduced and latent heat flux (out of the ocean) is increased. The amplitude of change is higher in the MPI case, corresponding to the higher SST change.

The Baltic Sea takes up heat from the atmosphere during the warm months and returns heat during wintertime. Both control runs confirm this picture. Under a warmer climate, atmosphere-to-ocean heat fluxes show a different distribution over the seasons. The ensemble mean heat loss is reduced between during winter, heat uptake is increased in April and heat uptake is reduced between May and July. By arriving of the summer, any additional net heat transfer into the ocean is counteracted by a negative feedback mechanism: the warm ocean responds with increased heat release by longwave outward radiation and latent heat. These signals are significant due to the length of experiments. Thus they cannot be explained as caused by interannual variability only. This general picture is a robust feature of all our experiments independent of the scenario (A2 or B2) and the driving global model (MPI or HC). Locally, in the northern part of the Baltic, heat fluxes change by up to 30 Wm^2 in the ensemble mean when strong ice cover changes (during spring) occur, and when the latent heat flux changes most (during fall).

The simulated mean annual maximum ice extent and the number of ice days in the control runs matches observations (SMHI & FIMR, 1982) for the period 1961 – 1990 well. Ice extent and volume (Tab. 1) are dramatically reduced in the scenarios. The ensemble mean reduction of ice volume is 83%. Corresponding to the SST changes, reduction is stronger for MPI and A2 scenarios. Large parts of the Bothnian Sea, the Gulf of Finland, the Gulf of Riga and the southwest archipelago of Finland are ice free in all scenarios. Severe ice winters do not occur anymore. However, sea ice is found in the Baltic in every single winter.

Some aspects of the simulated changes are contradictory within the ensemble, i.e. more uncertain than coherent findings. This is true for single months of the seasonal cycle of SST, certain secondary maxima in the seasonal cycle of surface warming and for the horizontal heat flux change pattern in the Baltic Proper. Sea surface salinity changes have not been discussed due to biases in precipitation (originating from the large scale circulation of global models) and the associated river runoff into the Baltic Sea. To overcome this problem, delta change experiments can be carried out (Meier and Kauker 2003), whereby the runoff and precipitation change is added on the recent observed forcing. In addition, the introduction of flux corrections for precipitation might be considered to enable salinity scenarios. Quality considerations with respect to the Baltic Sea climate projections are directly linked with processes of hemispheric and global scales. Thus improved GCMs are a precondition for major improvements of regional climate projections. Besides, clouds, radiation and turbulent heat fluxes are targeted for further improvement in the regional model. Even a model system with further improvements will contain uncertainties. Thus future efforts with large ensembles will be necessary to better quantify future climate uncertainty in the Baltic Sea.

References

Döscher, R., Willen, U., Jones, C., Rutgersson, A., Meier, H.E.M. & Hansson, U., 2002: The development of the coupled ocean-atmosphere model RCAO. *Boreal Env. Res*. 7, 183-192.

Döscher, R. & Meier, H.E.M., 2004: Simulated SST and heat fluxes in different climates of the Baltic Sea. *Ambio*, submitted.

Janssen, F., J.O. Backhaus & C. Schrum, 1999: A climatological dataset for temperature and salinity in the North Sea and the Baltic Sea. *Deutsche Hydrographische Zeitschrift*, Supplement 9, 245 pp

Jones C. G., Willén, U., Ullerstig, A. & Hansson, U. 2004. The Rossby Centre Regional Atmospheric Climate Model (RCA) Part I: Model climatology and performance for the present climate over Europe. *AMBIO* submitted.

Meier, H.E.M., Döscher, R. & Halkka A., 2004: Simulated distributions of Baltic sea ice in warming climate and consequences for the winter habitat of the Baltic ringed seal. *Ambio*, submitted.

Meier, H.E.M., Döscher R. & Faxen T., 2003: A multiprocessor coupled ice-ocean model for the Baltic Sea: application to salt inflow. *J. Geophys. Res*., 108 (C8), 3273

Meier, H.E.M. & Kauker, F. 2003: Sensitivity of the Baltic Sea salinity to the freshwater supply. *Clim. Res.*, 24, 231 - 242.

Nakicenovic, N., Alcamo, J., Davis, G., de Vries, B., Fenhann, J., Gaffin, S., Gregory, K., Grübler, A., et al., 2000. Emission scenarios. A Special Report of Working Group III of the Intergovernmental Panel on Climate Change. Cambridge University Press, 599 pp.

Räisänen, J., U. Hansson, A. Ullerstig, R. Döscher, L. P. Graham, C. Jones, H. E. M. Meier, P. Samuelsson & U. Willén, 2003: European climate in the late 21st century: regional simulations with two driving global models and two forcing scenarios. Climate Dynamics, published on-line 14 Nov 2003, DOI: 10.1007 / s00382-003-0365-x.

SMHI & FIMR, 1982: Climatological ice atlas for the Baltic Sea, Kattegat, Skagerrak and Lake Vänern (1963-1979). Norrköping, Sweden, 220 pp.

Limit cycles of the delayed action oscillator model for ENSO

A.V. Eliseev, D.V. Khvorostyanov, I.I. Mokhov and E.V. Sigaeva
A.M. Obukhov Institute of Atmospheric Physics RAS,
3 Pyzhevsky, 1091017 Moscow, Russia, e–mail: eliseev@ifaran.ru

Delayed action oscillator (DAO) currently is a wide–accepted model for the El Niño — Southern Oscillation (ENSO) process formation [4]. Here the limit cycles of the DAO model [1] are studied.

According to [3] the dimensionless formulation of the model is

$$dT/dt = \kappa T(t) - T(t-\tau) - [T(t) - rT(t-\tau)]^3 , \quad (1)$$

where T — east tropical Pacific sea surface temperature anomaly (from the climatological basic state), t — time, τ — delay, κ and r — constants.

Near–sinusoidal limit cycles with amplitude A and frequency ω can be found semianalytically using [2]. In this case Eq. (1) may be reduced to the transcedential equation for period $P = 2\pi/\omega$

$$\frac{\kappa - \cos\phi}{1 + r^2(2 + \cos 2\phi) - r(3 + r^2)\cos\phi} = \frac{\sin\phi - \phi/\tau}{r[(1 + r^2)\sin\phi - r\sin 2\phi]} \quad (2)$$

($\phi = \omega\tau$). Amplitude can be than found from

$$\frac{3}{4}A^2 = \frac{\kappa - \cos\phi}{1 + r^2(2 + \cos 2\phi) - r(3 + r^2)\cos\phi}. \quad (3)$$

Example of the solutions for the latter two equations is shown in Fig. 1. Generally these solutions can be found in a wider parameter region than the corresponding values obtained from the numerical integration of Eq. (1) (see, e.g., [3]). This is due to the limit cycle instability with respect to small perturbations in the difference of these two domains. For the stable limit cycles (when both numerically integrated periodic solutions of Eq. (1) and semianalytic solutions exist) the difference between numerically and semianalytically obtained values of amplitude and period is less than 10%.

Larger delay values lead to larger values both of oscillation period and amplitude. Larger values of κ result in larger A while P depends on κ only slightly.

This work is partially supported by the Russian Foundation for Basic Research and by the Russian President scientific grants.

References

[1] D.S. Battisti and A.C. Hirst. Interannual variability in a tropical atmosphere–ocean model: Influence of the basic state, ocean geometry and nonlinearity. *J. Atmos. Sci.*, 46(12):1687–1712, 1989.

[2] L. Cesari. Functional analysis and periodic solutions of non–linear equations. In *Contributions to Differential Equations*, volume 1, pages 149–187. Interscience Publ., New–York, 1962.

[3] I.I. Mokhov, A.V. Eliseev, and D.V. Khvorost'yanov. Evolution of the characteristics of interannual climate variability associated with the El Nino and La Nina phenomena. *Izvestiya, Atmos. Ocean. Phys.*, 36(6):681–690, 2000.

[4] J.D. Neelin, D.S. Battisti, A.C. Hirst, F.-F. Jin, Y. Wakata, T. Yamagata, and S.E. Zebiak. ENSO theory. *J. Geophys. Res.*, 103(C7):14261–14290, 1998.

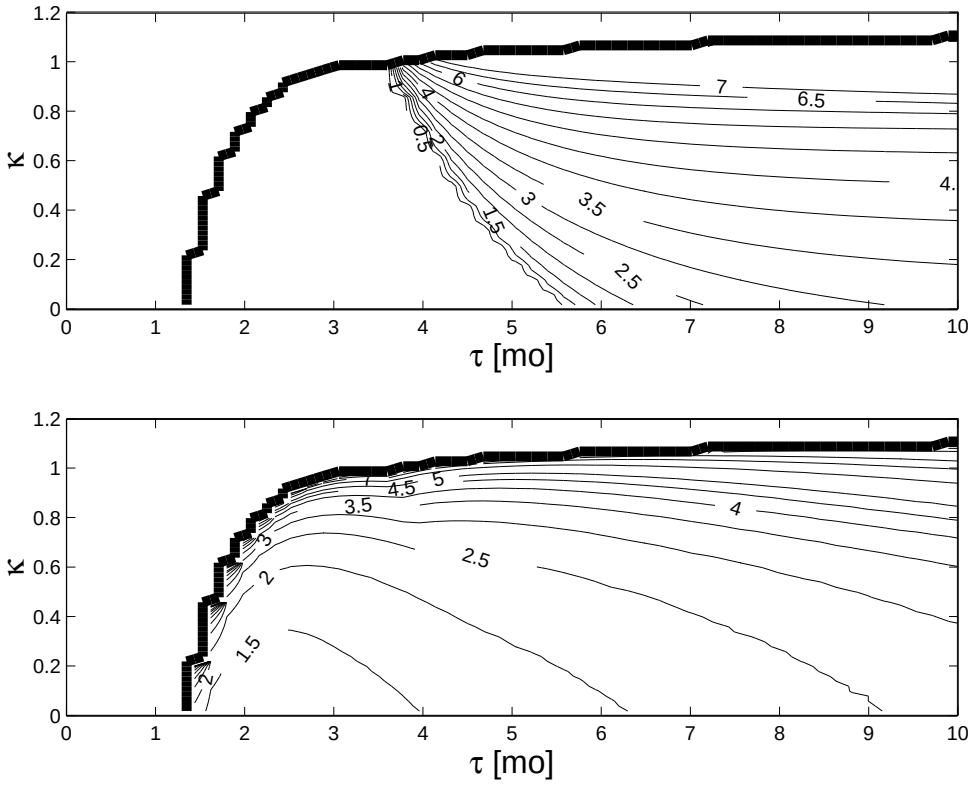

Figure 1: Dimensional amplitude (in Kelvins, upper panel) and period (in years, lower panel) obtained semianalytically for $r = 0.66$ [1]. Dimensional values are computed from the nondimensional ones using temperature and time scales 6.8 K and 3.6 mo respectively. Thick line borders the domain where solutions of Eqs. (2)–(3) exist.

Recent and ongoing climate modeling activities at UCL-ASTR

T. Fichefet, H. Goosse, E. Driesschaert, C. Poncin, and F. Wolk

Université Catholique de Louvain, Institut d'Astronomie et de Géophysique Georges Lemaître (UCL-ASTR), B-1348 Louvain-la-Neuve, Belgium, E-mail: fichefet@astr.ucl.ac.be.

Two simulations of the 21st century climate have been recently carried out at UCL-ASTR using, on the one hand, the UCL-ASTR climate general circulation model and, on the other hand, the same model coupled to a thermomechanical model of the Greenland ice sheet [*Huybrechts et al*., 2002]. Both simulations display a gradual global warming up to 2080. In the experiment that includes an interactive ice sheet component, a strong and abrupt weakening of the North Atlantic thermohaline circulation occurs at the end of the 21st century. This feature is triggered by an enhanced freshwater input arising mainly from a partial melting of the Greenland ice sheet. As a consequence of the circulation decline, a marked cooling takes place over eastern Greenland and the northern North Atlantic (Figure 1). This result underlines the potential role of the Greenland ice sheet in the evolution of climate over the 21st century. Further details about this study can be found in *Fichefet et al.* [2003].

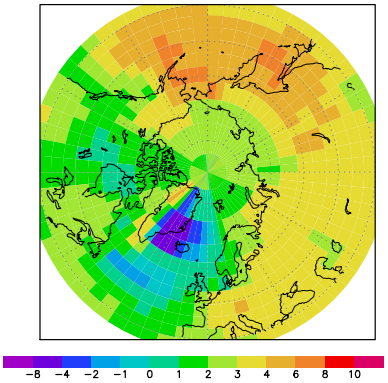

Figure 1. Changes in annual mean surface air temperature (in °C) by the end of the 21st century as simulated by the UCL-ASTR climate general circulation model coupled to a thermomechanical model of the Greenland ice sheet.

In additon, long simulations have been performed with ECBILT-CLIO, a three-dimensional atmosphere–sea ice–ocean model of intermediate complexity. On the basis of these experiments, we identified an interhemispheric climate lag mechanism, involving the long-term memory of deep water masses. Warm anomalies, formed in the North Atlantic when warm conditions prevail at the surface, are transported by the deep ocean circulation toward the Southern Ocean. There, the heat is released because of large-scale upwelling, maintaining warm conditions and inducing a lagged response of about 150 years compared to the Northern Hemisphere. Model results and observations covering the first half of the second millennium suggest a delay between the temperature evolutions in the Northern Hemisphere and in the Southern Ocean. The mechanism described here provides a reasonable hypothesis to explain such an interhemipsheric lag [*Goosse et al.*, 2003].

A three-dimensional Earth system model of intermediate complexity has also been developed. This model, called LOVECLIM, consists of a quasi-geostrophic atmospheric model (ECBILT), a sea ice–ocean general circulation model (CLIO), a dynamical model of the biosphere and of its carbon content (VECODE), an oceanic carbon cycle model (LOCH), and thermomechanical models of the Greenland and Antarctic ice sheets (AGISM). This work was done in close collaboration with the Departement Geografie of the Vrije Universiteit Brussel, Brussels, the Laboratoire de Physique Atmosphérique et Planétaire of the Université de Liège, Liège, and the Potsdam-Institut für Klimafolgenforschung, Potsdam. The coupled model is being validated by conducting ensemble runs over the last 500 years driven by natural and anthropogenic forcings, and by comparing outputs to historical and proxy data available. In the future, it will be used to investigate the evolution of climate and sea level over the third millennium, and in particular, to explore the thresholds for abrupt climate change during this period. This model (without the LOCH and AGISM components) is also presently utilized to understand the climate changes that occurred during the Holocene (last 9,000 years) within the European project "Models and observations to test climate feedbacks (MOTIF)", which is part of the Paleoclimate Modeling Intercomparison Project (PMIP).

Acknowledgments. T. Fichefet and H. Goosse are Research Associates at the Belgian National Fund for Scientific Research. This work is performed within the scope of the Second Multiannual Scientific Support Plan for a Sustainable Development of the Belgian State and the Environment and Sustainable Development Programme of the European Commission.

References

Fichefet, T., C. Poncin, H. Goosse, P. Huybrechts, I. Janssens, and H. Le Treut, Implications of changes in freshwater flux from the Greenland ice sheet for the climate of the 21st century, *J. Geophys. Res., 30 (17), 1911*, doi: 10.1029/2003GL017826, 2003.

Goosse, H., V. Masson-Delmotte, H. Renssen, M. Delmotte, T. Fichefet, V. Morgan, T. van Ommen, B.K. Khim, and B. Stenni, A late medieval warm period in the Southern Ocean as a delayed response to external forcing?, *Geophys. Res. Lett*., submitted, 2003.

Huybrechts, P., I. Janssens, C. Poncin, and T. Fichefet, The response of the Greenland ice sheet to climate changes in the 21st century by interactive coupling of an AOGCM with a thermomecanical ice sheet model, *Ann. Glaciol*., *35*, 409-415, 2002.

International Stretched-Grid Model Intercomparison Project (SGMIP): Initial Results on 12-year Regional Climate Simulations with Variable-Resolution GCMs

Michael Fox-Rabinovitz, University of Maryland, U.S.A.
Jean Cote, RPN/Environment Canada, Canada
Michel Deque, Meteo-France, France
Bernard Dugas, RPN/Environment Canada, Canada
John McGregor, CSIRO, Australia

The international Stretched-Grid Model Intercomparison Project (SGMIP) has been initiated for studying the new emerging global variable-resolution/stretched-grid approach to regional climate modeling.

The variable-resolution stretched-grid (SG) GCMs have been developed and successfully tested in the straightforward simulation mode (like that used for a typical atmospheric GCM) during the mid-late 90s. The SG-GCMs are the variable-resolution versions of the basic GCMs of the following four major meteorological centers/groups: the Meteo-France, ARPEGE model, the RPN/Canadian Meteorological Centre, GEM model, the Australian CSIRO C-CAM model, and the U.S. NASA/GSFC GEOS model. The regional climate simulation results obtained with the SG-GCMs have shown the maturity of the SG-approach. There is a consensus among the groups involved in the SG-GCM developments on the necessity of the model intercomparison at this stage of experimentation with the models. The intercomparison is focused on the following major scientific and computational issues: stretching strategies; approximations of model dynamics; treatment of model physics including its calculation on intermediate uniform resolution or directly on stretched grids; multi-model ensemble calculations; consistent regional-to-global scale interactions; optimal performance on parallel supercomputers.

The total number of global grid points for the SG-GCMs is (or close to) that of the 1º x 1º uniform grid. The area of interest is (or close to) the major part of North America: 20º – 60º N and 130º – 60º W. The regional resolution is about 0.5º. The surface boundary forcing (SST and sea ice) is used at 2º x 2.5º or 1º x 1º resolution. The 12-year period chosen for model simulations includes the recent ENSO cycles.

The existing reanalysis data as well as independent data like high-resolution gauge precipitation and high-resolution satellite data, are used for the SG-GCMs validation.

The 12-year SG-GCM simulations are analyzed in terms of studying: the impact of resolution on efficient/realistic downscaling to mesoscales; ENSO related and other anomalous regional climate events (floods, droughts, etc.) and major monsoonal circulations at mesoscale resolution; water and energy cycles; and global impacts.

The SG-approach allows studying not only downscaling but also up-scaling effects. Analyzing multi-model ensemble integrations is one of the focal points of SGMIP. The multi-model ensemble results for global and regional fields are presented at: http://essic.umd.edu/~foxrab/sgmip.html

The experience obtained with SGMIP will allow us to make a meaningful connection to AMIP-2 in terms of consistent regional-to-global scale climate studies.

Our joint SGMIP effort, focused on a better understanding of the SG-approach, is beneficial to all the participants as well as to a broader regional and global climate modeling community.

Simulation of impact of deforestation in African and north-east Indian region on Asian summer monsoon using CCM3 model

A.Gupta*, P.K.Thapliyal, P.K.Pal
Atmospheric Sciences Division
Meteorology and Oceanography Group
Space Applications Center
Indian Space Research Organisation
INDIA

***email-id: anju_30sept@yahoo.com**

The fact of rapid deforestation has been one of the major concerns since last decade. In India, the forest cover of the country has been declining since last several years. The impact of these changes on Indian monsoon is still an open question.

In this work, an attempt has been made to address this question with the National Center for Atmospheric Research (NCAR) Community Climate Model (CCM3.6). The T42 version of CCM3 with a horizontal resolution of 2.8°x2.8° is used for this study.

The influence of deforestation is modeled by the changes in the surface parameters such as land cover. The changes are made over the African Region and some parts of North-East Indian Region. The consequences of the changes in land cover are the changes in surface albedo, ground wetness, surface roughness etc.

The standard T42 version of NCAR Community Climate Model (CCM3) which includes LSM as a coupled model is integrated for five years, for the control run. Further the impact of deforestation have been studied for three different scenarios. The model is integrated for five years with forest cover replaced by grassland in three different classes, viz. 100%, 50%, 25%. The spatial extent of the change is 0-120°E, 20°S-50°N. Based on the model simulations for five years in three different scenarios i.e 25%, 50% and 100% deforestation, following conclusions are drawn:-

- Wind vector fields at 850mb shows that circulation has been strengthened in Arabian Sea whereas weakened in Bay of Bengal. Due to deforestation, circulation has weakened in Indian subcontinent, Africa and north-east India. Somali Jet has also weakened.
- Wind vector fields at 200mb gives the indication that deforestation will affect the anticyclonic structure over Tibet in the upper level.
- There is considerable decrease in rain rate over Africa, north-east India, Burma and over Indian Ocean whereas over India, spatial distribution of rain rate is expected to change due to deforestation. Over northern India, rain rate has decreased whereas over southern part, it will increase. Also, over Arabian sea and Bay of Bengal, rain rate has increased up to 5mm/day.
- Over north-east India and Burma region (where forest cover was removed completely), surface temperature has increased. Over land portion of India, surface

temperature is shown to have decreased by 1°K. Over southern belt of Africa 10°S-10°N, surface temperature has increased by 7°K, whereas over northern belt 10-20°N, it has decreased by 3°K. Due to deforestation, deserts are expected to have higher surface temperature and chance of more desertification.

- Model is showing sensitivity to land surface changes. It is evident from the gradual deforestation simulation comparisons. We can see that rain rate is decreasing as we go from 25% to 100% deforestation over the selected regions.

The impact of small scale changes in land cover could not be resolved by these experiments due to 2.8°x2.8° resolution of the model. Further experiments need to be done with high resolution regional climate model to study the impact of local changes in land cover.

The following figure shows the difference in JJA rain rate due to 100% deforestation in the African and north-east Indian region.

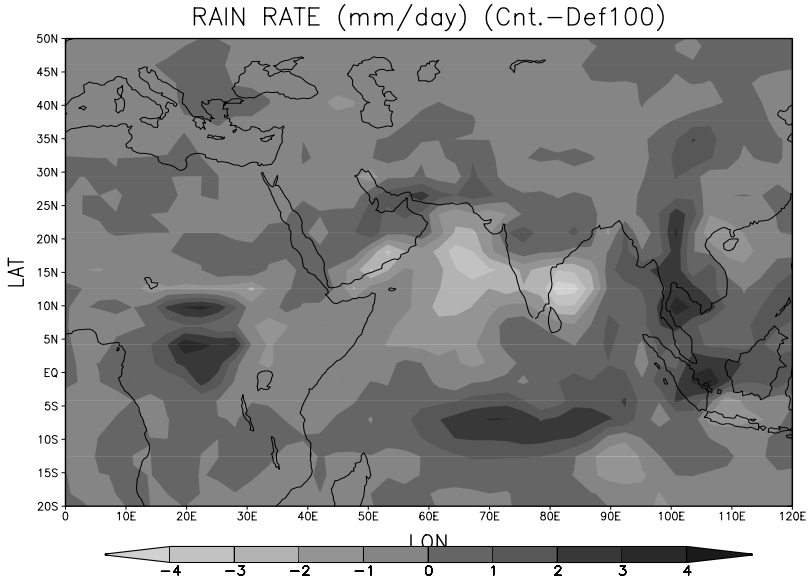

The surface climatology simulated by the Canadian Regional Climate Model (CRCM)

Yanjun Jiao[1], Daniel Caya[2] and Rene Laprise[1]

1. Department of Earth and Atmospheric Sciences,
University of Quebec at Montreal, Montreal, Quebec, Canada
2. Consortium Ouranos, Montreal, Quebec, Canada
email: jiao.yanjun@uqam.ca

The third generation of the Canadian Regional Climate Model (CRCM) (Caya and Laprise 1999) is evaluated through the comparisons with observed surface climatology. In this experimental configuration, the model domain (fig. 1) covers the entire Canadian territory and most of the United States with a total of 193x145 polar stereographic grid points at a 45km horizontal resolution and 29 Gal-Chen levels in the vertical. The model is nested by the one-way nesting method of Davies (1976) with 9 grid points in the sponge zone. The initial and lateral boundary conditions come from NCEP/NCAR re-analysis data and the surface forcings are prescribed with observed monthly mean sea surface temperature (SST) and sea ice concentration (SIC) from the Atmospheric Model Intercomparison Project (AMIP II). The simulation was started on January 1, 1987 and was run continuously for 5 years with 15-minute time steps. To prevent CRCM's large-scale deviate from its driving fields in the long-term simulation, a new spectral nudging technique is also introduced in this version of the model (Denis et al. 2002).

The monthly and seasonal mean results from the model's last four years of simulation were compared with observed screen surface temperature from the Climate Research Unit (CRU; New et al. 2000) and with global precipitation data (Xie and Arkin, 1996). Model results were also compared with the output from the CRCM's previous generation (Laprise et al, 2003).

Fig. 2 shows the domain-averaged monthly mean screen temperature over all land grid points between 30°N and 70°N latitudes. The agreement between CRCM simulation and CRU observation is quite good. The CRCM simulates very well the seasonal variability of screen temperature over the main continent of North America. Compare with the CRU observation, the model only shows a warm bias of less than 1°C during the warm seasons and the cold bias in winter seasons not more than 3°C.

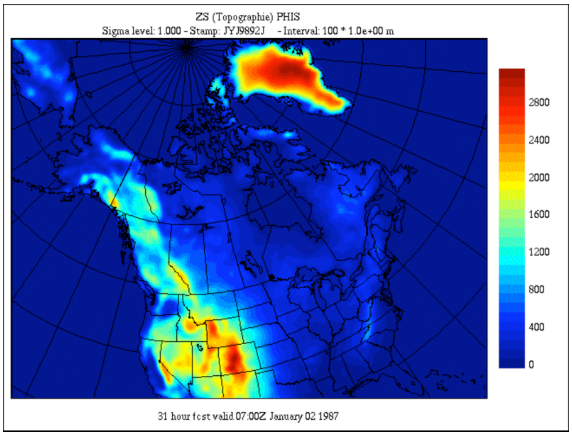

Fig. 1. CRCM model domain and topographic field (in meters).

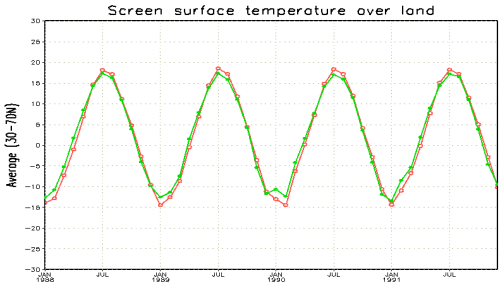

Fig. 2. Domain-averaged monthly mean screen temperature over main continent of North America (30°-70°N). (The red line with open circles is the CRCM simulation and the green line with dots is the CRU observation)

The seasonal precipitation simulated by the CRCM is consistent with Xie-Arkin observational data. For example, in winter (DJF) (Fig. 3), most of the land precipitation produced by the CRCM is right concentrated in a very narrow band along the West Coast, from Alaska to British Columbia, and reaching the Washington and Oregon states. Another broader precipitation zone is located over southeastern United States. Over the Western Pacific ocean and Northern Atlantic ocean, the precipitation pattern and amounts simulated by the CRCM are also in good agreement with observational data.

Finally, the comparison between the CRCM's second and third generation reveals that the model's performance has greatly improved (not shown).

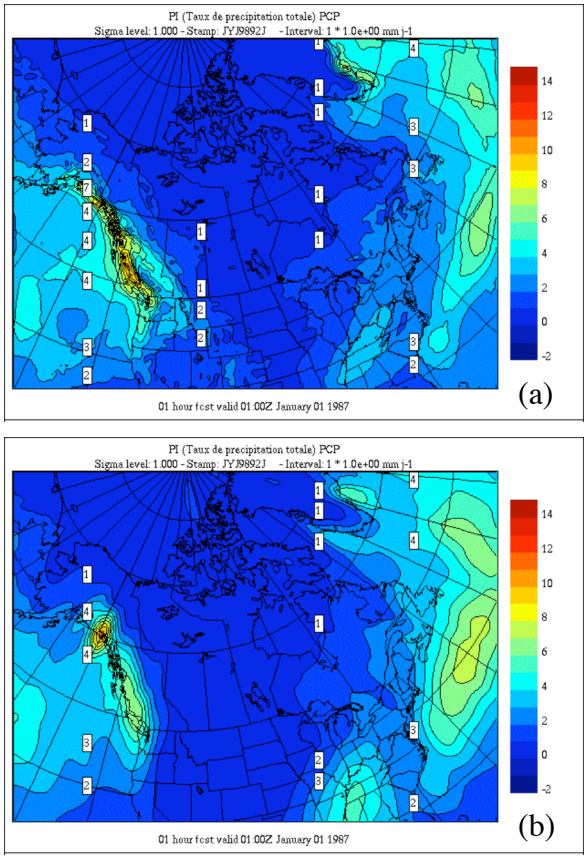

Fig. 3. Winter (DJF) mean precipitation rate (mm/day)(a) simulated by CRCM and (b) from Xie-Arkin observations. (9 grid points sponge zone is not included)

References:

Caya, D., and R. Laprise (1999). A semi-implicit semi-Lagrangian regional climate model: The Canadian RCM. Monthly Weather Review **127**(3): 341-362.

Davies, H. C. (1976). A lateral boundary formulation for multi-level prediction models. Quarterly Journal of the Royal Meteorological Society **102**: 405-418.

Denis, B., J. Côté, and R. Laprise (2002). Spectral decomposition of two-dimensional atmospheric fields on limited-area domains using the discrete cosine transform (DCT). Monthly Weather Review **130**(7): 1812-1829.

Laprise, R., D. Caya, A. Frigon, and D. Paquin. (2003). Current and perturbed climate as simulated by the second-generation Canadian Regional Climate Model (CRCM-II) over northwestern North America. Climate Dynamics **21**(5-6): 405 – 421.

New, M., M. Hulme, et al. (1999). "Representing Twentieth-Century Space-Time Climate Variability. Part I: Development of 1961-90 Mean Monthly Terrestrial Climatology." Journal of Climate **12**: 829-856.

Xie, P., and P. A. Arkin (1996). Analyses of global monthly precipitation using gauge observations, satellite estimates, and numerical model predictions. Journal of Climate **9**: 840-858.

Regional Climate Prediction by using a Japan Meteorological Agency Nonhydrostatic Model with a High Resolution. Part 1: Outline/Purpose of a High-Resolution Long-Term Prediction

Teruyuki KATO[1], Kazuaki YASUNAGA[2], Chiashi MUROI[1], Masanori YOSHIZAKI[1], Sachie KANADA[2], Akihiro HASHIMOTO[2], Yasutaka WAKAZUKI[2], Hisaki EITO[1], Syugo HAYASHI[1], Hidetaka SASAKI[1]

[1]*Meteorological Research Institute / Japan Meteorological Agency, Tsukuba*
[2]*Advanced Earth Science and Technology Organization, Tokyo*

1. Introduction

We are trying to predict a regional climate around Japan Islands using a high-resolution nonhydrostatic model at the time of global warming. In East Asia, summer monsoon starts from the south in May, and ends in July, extending to the north. This monsoon produces the rainy season, called Baiu season in Japan, in East Asia. It also produces the frontal zone, called Baiu frontal zone in Japan, in the front of the Continental high pressure. Our motivation is to examine how the position of the Baiu frontal zone and the intensity of the precipitation forming over the frontal zone are changed by global warming, and finally we want to contribute to IPCC.

As the first step, we are verifying the accuracy of the present regional climate that is predicted by using regional analyses of Japan Meteorological Agency (JMA) as initial and boundary conditions. Next, we have a plan to predict the present regional climate by giving boundary conditions produced from the prediction of a global climate model, and we also have to compare the predicted precipitation areas and intensity, depending on the horizontal resolution. As the final step, we will examine the regional climate at the time of global warming by using the predictions of a global climate model.

2. Numerical Model

We have applied a nonhydrostatic model developed jointly by the Meteorological Research Institute and Numerical Prediction Division, JMA (Saito et al., 2001, JMA-NHM) to clarify the mechanisms of mesoscale convective systems. The model horizontal resolution of 1-5 km has been used, and the integration time has been less than 1 day. Therefore, to use JMA-NHM as a regional climate model, we had to make some improvements, and ascertain its stability for a long-term integration.

For a long-term integration, we must prepare a huge amount of boundary condition datasets, and restart the integration repeatedly due to the restrict ion of computation system. All of boundary condition datasets had to be necessary for its restarting. At first, we improved JMA-NHM to restart the integration with the minimum required datasets. We also improved JMA-NHM to nest sea surface temperature. We introduced the spectral boundary coupling (SBC) method to JMA-NHM to take in large scale effects (the explanation of SBC method is seen in Part 2).

*Corresponding author address: Teruyuki Kato, Meteorological Research Institute, 1-1 Nagamine, Tsukuba, Ibaraki 305-0052 Japan: e-mail: tkato@mri-jma.go.jp

Horizontal resolution: 5km (5km-NHM)
Vertical layers (distances): 48 layers (20m near the surface to 920m at the model top)
Basic equations: Full compressible system
Treatment of sound waves: Horizontally explicit and vertically implicit (HE-VI)
Vertical coordinate: Terrain following
Turbulent closure: Level 2.5
Boundary condition: Rayleigh damping is used for lateral and upper boundaries. SBC method is applied to upper level from 500hPa.
Cloud Microphysics: 3ice＋2 moments (Number densities of all hydrometeors are predicted.)
Convective parameterization: none
Advection: Second order in conjunction with modified advection scheme
Radiation: Cloud amount is determined by relative humidity.
Surface temperature: 4 layer model

The major specifications of JMA-NHM used as a regional climate model are shown in Table 1. The horizontal resolution is set to 5km (5km-NHM), because this grid size had been able to reproduce the heavy rainfall events during the Baiu season. However, we want to up to 2km at the final stage.

3. Experiment Designs at the First Stage

The initial and boundary datasets are produced from the 6-hourly regional analyses of JMA. The integration starts from 20 June, 2001, 2002, and 2003, and its period, including the Baiu season, is 70 days for each year. The model domain and orography are shown in Fig. 1. We also use a JMA-NHM with a 20 km horizontal grid (20km-NHM) to compare the effect of resolution. For 20km-NHM, the moist convective adjustment is used in conjunction with microphysics, and the other specifications are the same as those of 5km-NHM.

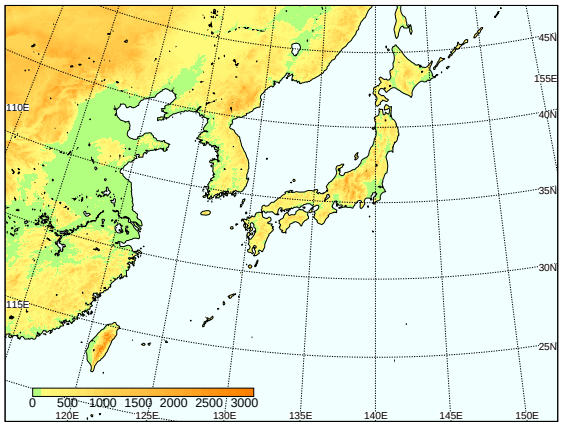

Fig. 1 The model domain and orography.

4. Current Results

Figure 2 shows the observed and predicted 12-hour rainfall after the integration of 5 days. The observed rainfall is estimated by JMA operational radar and ground observation data. The heavy rainfall areas are observed over Kyushu and Shikoku areas. These areas are well reproduced by 5km-NHM, but not for 20km-NHM. This indicates that a high-resolution regional climate model is necessary to predict local heavy rainfalls.

Figure 3 shows the accuracy of 5km-NHM predicted sea level pressure (SLP). During the whole integration period, the differences of the maximum and domain averaged SLP are less than a few hPa. However, the minimum predicted pressure does not decrease to less than 960 hPa. The minimum analyzed pressure less than 960 hPa was produced by typhoons. Since the grid size of 5km can not resolve the eye wall of typhoons, the warm core in the eye that induces the decrease of pressure can not be reproduced. Therefore, at least the grid size of 1km is necessary to predict the accurate minimum pressure.

These results indicate that 5km-NHM has a good accuracy to be used as a regional climate model. Now, we are also verifying the other predicted variables, e.g., near-surface temperature and relative humidity, and rainfall. The results of these verifications may require us to make further improvements of JMA-NHM. Moreover, we plan to estimate Q1 and Q2 (apparent heat source and moisture sink) from the output of 5km-NHM, and want to make new suggestions to convective parameterization.

Acknowledgements

This study is conducted by the fund of Research Revolution 2002, and the numerical calculations are made by NEC SX-6 on Earth Simulator.

Refferences

Saito, K., T. Kato, H. Eito and C. Muroi, 2001: Documentation of the Meteorological Research Institute / Numerical Prediction Division Unified Nonhydrostatic Model. *Tech. Rep.of MRI*, **42**, p133.

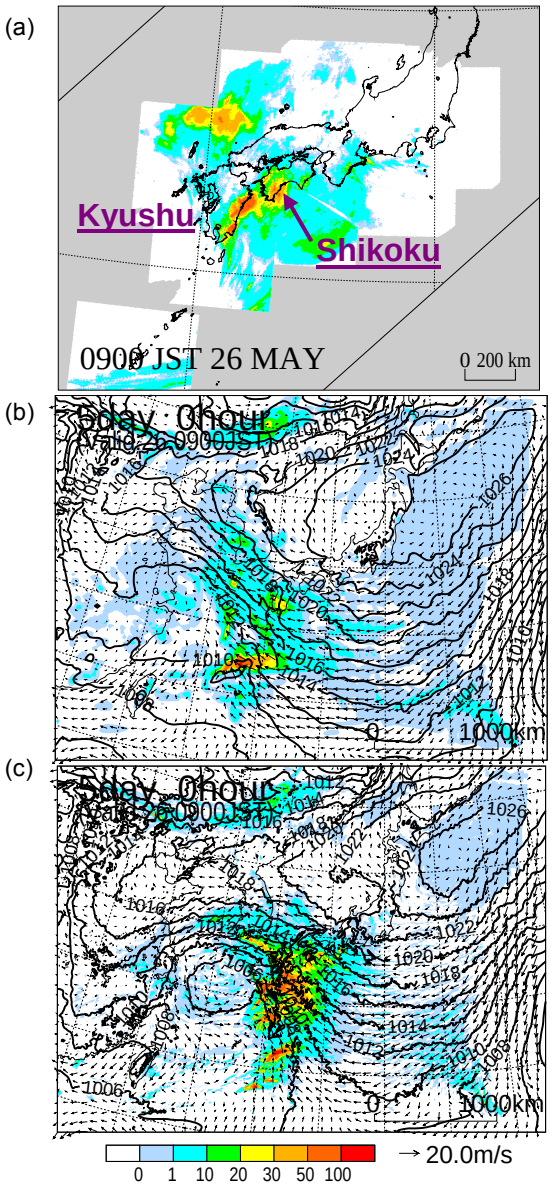

Fig. 2 (a) Observed 12-hour rainfall at 09 JST on 26 May 2003, (b) 20km-NHM and (c) 5km-NHM predicted rainfall and sea level pressure.

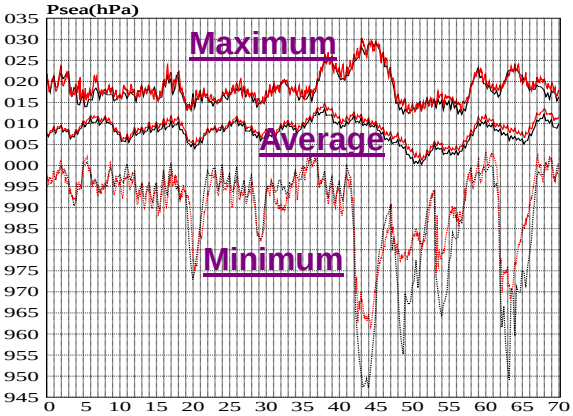

Fig. 3 Time series of the maximum, minimum, and domain averaged sea level pressure of analyses (black lines) and 5km-NHM prediction (red lines) in 2002.

51-year Simulation of the Period from 1951 to 2001 by the JMA AGCM

By Shoji KUSUNOKI, Keiichi MATSUMARU, Toshiyuki NAKAEGAWA, Isamu YAGAI and Osamu ARAKAWA

Climate Research Department, Meteorological Research Institute, Japan Meteorological Agency, 1-1 Nagamine, Tsukuba, Ibaraki 305-0052, JAPAN, E-mail：skusunok@mri-jma.go.jp

1. Introduction: We have evaluated the climate variations and changes over the 51-year period from 1951 to 2001 simulated by the Japan Meteorological Agency (JMA) Atmospheric General Circulation Model (AGCM). The numerical experiments were conducted under the framework of the Climate of the 20th Century International Project (C20C, http://grads.iges.org/c20c/). Model's ability to reproduce linear trend and year-to-year variability of land-surface air temperature and land-only precipitation were investigated for all four seasonal means and annual mean field.

2. Model: The model called MJ98 (Shibata et al. 1999) was originally used for operational numerical weather forecasting and were later modified for climate research usage. The model has a spectral resolution of triangular truncation at wave number 42 (T42), corresponding to about 270 km horizontal grid spacing. It has 30 vertical levels with top at 0.4 hPa. For cumulus convection, a prognostic Arakawa-Schubert scheme is used. For Land surface processes, a Simple Biosphere scheme (SiB) is used.

3. Experimental design: Six-member ensemble integrations were performed from 1951 to 2001, forcing with the observed Sea Surface Temperature (SST) and sea ice data "HadISST1" by Rayner et al. (2003). As for greenhouse gases, the observed concentration of carbon dioxide CO_2 adapted from Hansen et al. (2002), increasing from 311 ppmv in 1951 to 370 ppmv in 2001, was given homogeneously to the whole atmosphere without any seasonal cycle. The concentration of both CH_4 (1650 ppbv) and N_2O (306 ppbv) are kept constant in time and space.

4. Validation data: Land-surface air temperature is validated using the variance adjusted observational data "CRUTEM2v" by Jones et al. (2001) for the 51-year period from 1951 to 2001. Land-only precipitation is validated using the observational data by Hulme et al. (1998) for the 47-year period from 1951 to 1997. Both observational data are based on monthly mean at 5-degree longitude-latitude box.

5. Trend: Figure 1 shows the time series of summer land-surface air temperature anomaly averaged for the Northern Hemisphere. Model reproduces observed positive trend, although the magnitude of trend is underestimated. Figure 2 shows the time series of summer land-only precipitation ratio averaged for the Northern Hemisphere. Model well reproduces observed negative trend.

6. Year-to-year variability: Model's ability to simulate year-to-year variability of land-surface air temperature was investigated by calculating the temporal correlation coefficient between observed temperature and simulated temperature. Correlation coefficient between two time series in Fig. 1 is very high at 78.8, but it reduces to 69.0 if linear trends are excluded from these two time series. Similarly, correlation coefficient between two detrended time series in Fig. 2 reduces to 45.0.

References

Hansen et al., 2002: Climate forcings in Goddard Institute for Space Studies SI2000 simulations. *J. Geophys. Res.*, **107**(D18), 4347, doi:10.1029/2001JD001143.

Hume et al., 1998: Precipitation sensitivity to global warming: Comparison of observations with HadCM2

simulations. *Geophys. Res. Letts.*, **25**, 3379-3382.

Jones et al., 2001: Adjusting for sampling density in grid box land and ocean surface temperature time series. *J. Geophys. Res.*, **106**(D4), 3371-3380.

Rayner et al., 2003: Global analyses of sea surface temperature, sea ice, and night marine air temperature since the late nineteenth century. *J. Geophys. Res.*, **108**(D14), 4407, doi:10.1029/2002JD002670.

Shibata et al., 1999: A simulation of troposhpere, stratosphere and mesosphere with an MRI/JMA98 GCM. *Papers in Meteorl. and Geophys.*, **50**, 15-53.

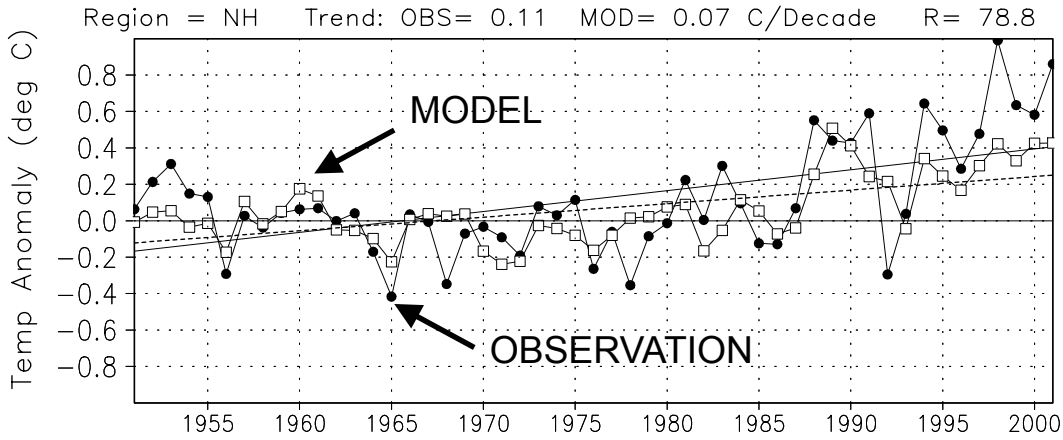

Fig. 1. Time series of summer mean (June - August) land-surface air temperature anomaly (°C) averaged for the Northern Hemisphere (2.5-87.5 °N) from 1951 to 2001. Anomalies are relative to 1961-1990 climatology. Black circle ● indicates observation by Jones et al. (2001). The slant solid line is the linear regressed line by least square fitting to observed time series. White square □ indicates ensemble average of model simulations. The dashed line is the linear regressed line for model. Values of observed trend (OBS) and model trend (MOD) are shown at the top outside the panel by the unit °C/decade. The value of R in the top-right corner outside the panel denotes the temporal correlation coefficient (%) between two time series. R reduces to 69.0, if linear trends are excluded from these two time series.

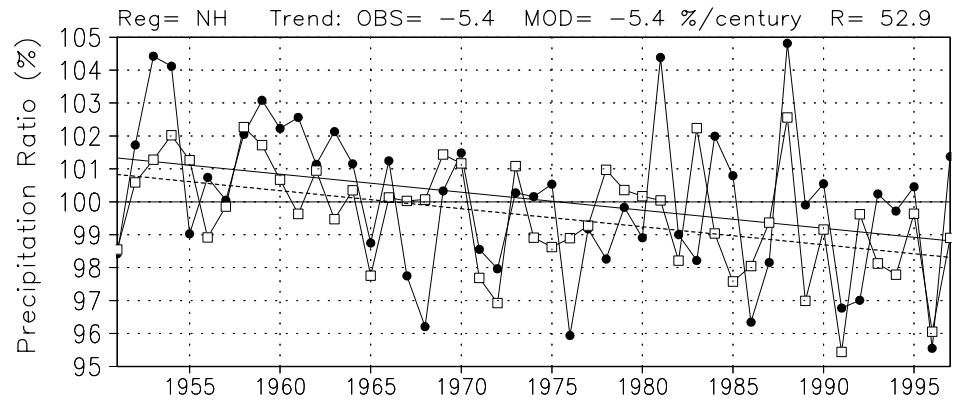

Fig. 2. Same as Fig. 1, but for land-only precipitation ratio (%) to the 1961-1990 climatology. Note that time series end in 1997 owing to the limitation of observational data adapted from Hume et al. (1998). Trend unit is %/century. The value of R reduces to 45.0, if linear trends are excluded from these two time series.

Changes in winter cyclone vertical structure with increasing CO_2

Eun-Pa Lim and Ian Simmonds
School of Earth Sciences
The University of Melbourne
Victoria 3010, Australia
E-mail: eplim@earthsci.unimelb.edu.au

In a warmer globe caused by increasing CO_2, it is expected that lower tropospheric baroclinicity will decrease while upper tropospheric baroclinicity increases (Zhang and Wang 1997). In order to find out how these different patterns of baroclinicity change in the troposphere affect extratropical cyclones, we investigate the 'vertical organization' of extratropical cyclones with NCEP-DOE reanalysis-II winter (DJF in the NH, JJA in the SH) data (1979-2000) and CSIRO MARK2 atmosphere-ocean coupled GCM data produced according to IPCC IS92a scenario (Wu et al. 1999). For an appropriate comparison between these data sets, we base our analysis on 22 years from the NCEP2, CSIRO Mark2 control run, and the transient 2xCO_2 and 3xCO_2 runs.

The Melbourne University cyclone finding and tracking scheme (Simmonds and Keay 2000) is used to detect cyclones at mean sea level (msl), 925, 850, 700, 600 and 500 hPa geopotential heights (hereafter Z*pressure*). The vertical organization over surface cyclones is determined in a series of steps: First, we find the location and time of maximum depth of a surface cyclone. In a circle of 4° latitude radius centered on the location and the time found, we search for the vertical extension of the cyclone at the next data level. This tracking is continued to Z500.

We find from our "vertical tracking" that about 41% and 36% of surface extratropical cyclones have well organized vertical structure in that they can be traced all the way to Z500 in winter in the NH and SH, respectively. Furthermore, this percentage has increased over our 22 years of observational record (Figure 1), but only the trend in the SH is significantly different from zero at the 99% confidence level (c.l.).

The surface cyclone features show clear differences according to whether or not surface cyclones are vertically well organized. The surface cyclones having a Z500 cyclone partner are more intense, larger and deeper than those ending their connection at Z700 or lower. Moreover, the mslp-Z500 coupled cyclones have about twice the lifespan of the others (not shown).

When surface cyclones experience their deepest stages, the average distance between Z500 and mslp cyclone centers is about 388 km and 384 km in winter in the NH and SH, respectively. This distance has reduced for the last two decades, and these decreases are -1.74 and -1.96 km per annum (99% c.l.) in the NH and SH (Figure 2). It might imply that cyclones have become more barotropic at the full development stage over the last 22 years.

About 43% and 50% of the control model cyclones have vertically well organized structure up to Z500 in the NH and SH, respectively (Table 1). With increasing CO_2, the ratio of cyclones having well organized vertical structure increases, and the mean separation of msl-Z500 pairs is seen to decrease.

In conclusion, the results of vertical organization of cyclones in the CSIRO simulations are consistent with those in NCEP2. Therefore, some of present changes in cyclone vertical structure seem to be following the patterns possibly cyclones experience in the warmer world.

Kanamitsu, M., and coauthors, 2002: NCEP-DOE AMIP-II Reanalysis (R-2). *Bull. Amer. Meteor. Soc.*, **83**, 1631-1643

Simmonds, I. and Keay, K., 2000: Mean Southern Hemisphere extratropical cyclone behavior in the 40-year NCEP-NCAR reanalysis. *J. Climate*, **13**, 873-885

Wu, X., Budd, W.F. and Jacka, T. H. 1999: Simulations of Southern Hemisphere warming and Antarctic sea-ice changes using global climate models. *Ann. Glaciol.*, **29**, 61-65

Zhang, Y. and Wang, W.-C., 1997: Model-simulated northern winter cyclone and anticyclone activity under a greenhouse warming scenario. *J. Climate*, **10**, 1616-1634

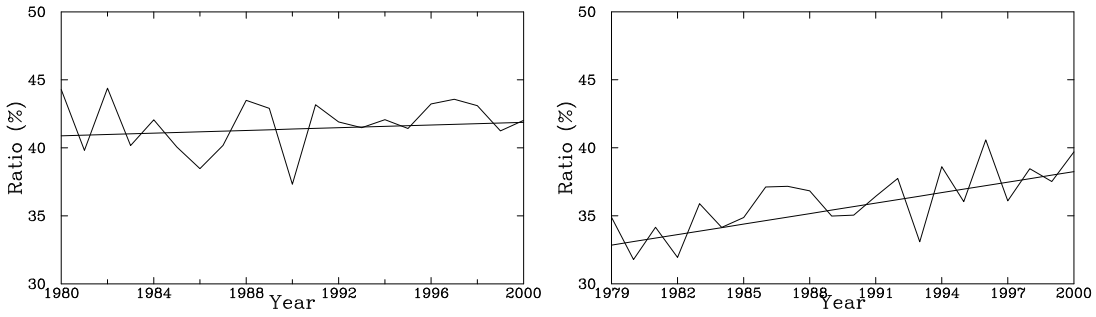

(a) (b)

Figure 1: Time series of the ratio of the number of well-organized cyclones to the entire mslp extratropical cyclones in winter seasons in 1979-2000. (a) NH and (b) SH

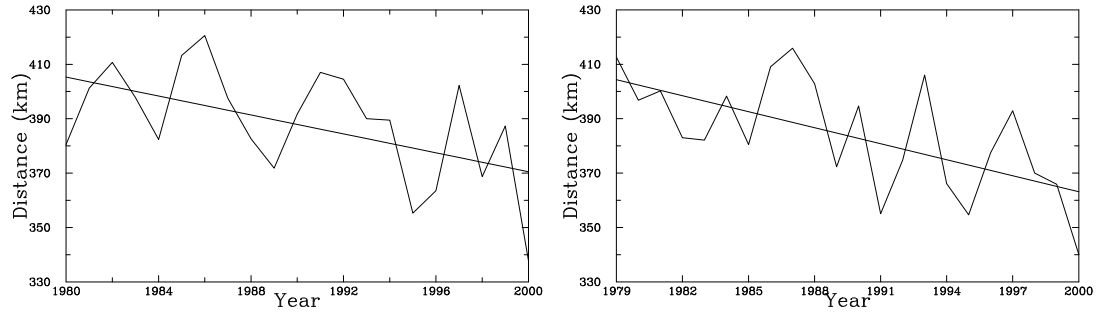

(a) (b)

Figure 2: Time series of the average distance between coupled Z500 and mslp cyclone centers. (a) NH and (b) SH

		CONT	2xCO_2	3xCO_2
Ratio	NH	42.6	43.3	45.1
(%)	SH	49.8	50.8	51.6
Distance	NH	505.7	494.1	485.8
(km)	SH	450.0	441.7	428.5

Table 1: Changes of vertically well structured cyclones according to CO_2 concentration in the control run (CONT) and transient runs (2xCO_2, 3xCO_2).

A Ten-year Climatology of the Summer Monsoon over South China from a Regional Climate Model

YIMING LIU* AND JOHNNY C L CHAN
Laboratory for Atmospheric Research, Department of Physics & Materials Science
City University of Hong Kong, Hong Kong, China
*E-mail: yimliu@163bj.com

1. Introduction

The summer monsoon over South China (SC) and the South China Sea (SCS) is an important component of the East Asia summer monsoon (Ding and Li 1999; Lau et al. 2000). A regional climate model has been developed at City University of Hong Kong based on a modified version of RegCM2 at the China National Climate Center (Ding et al. 2000). The model (RegCM) has been tested and found to be able to simulate to a large extent the precipitation over SC and the SCS for the months of May and June (Chan et al. 2003). To study the interannual variability of the summer monsoon over these regions, it is necessary to establish a model climatology to serve as a comparison and to remove any systematic model biases.

2. The model and initialization

The model is initialized on April 1 and integrated up to the end of July for the 10 years 1991-2000. Initial and boundary conditions used in this study are from the NCEP/NCAR reanalysis data. Lateral boundary conditions are updated at 6-hourly intervals. The sea surface temperature data are taken from the NCAR weekly optimum interpolation SST version 2 with a 1°latitude × 1°longitude spatial resolution. The model has 16 vertical levels, a 60-km horizontal resolution and a domain size of 125×155 grid points (Fig. 1), and the model top is at 10 hPa.

3. Results

Preliminary analyses suggest that the model is capable of reproducing the major characteristics in the regions of interest. The 500-hPa geopotential heights averaged between May and July 1991-2000 simulated by RegCM show basic features similar to those observed (Fig. 2), including the western Pacific subtropical high and the trough over the Bay of Bengal. The main error is the simulated trough over the Bay of Bengal being too strong than the observed. The model can also simulate the main moisture transport over the Bay of Bengal at 850 hPa (Fig. 3) although the magnitudes over the Bay of Bengal and SC (SCS) are stronger (weaker) than those observed.

The interannual variability of rainfall, wind fields, moisture transport and other parameters relevant to the summer monsoon over SC and the SCS are currently being analyzed.

Acknowledgments. This research is sponsored by the Research Grants Council of the Hong Kong Special Administrative Region of China Grant CityU 2/00C.

References

Chan, J. C. L., Y. Liu, K. C. Chow, Y. Ding, W. K. M. Lau and K. L. Chan, 2003: Design of a regional climate model for the simulation of South China summer monsoon rainfall. *Submitted to J. Meteor. Soc. Japan.*

Ding, Y. H., and C. Y. Li (Eds.), 1999: *Onset and Evolution of the South China Sea Monsoon and Its Interaction with the Ocean*. Chinese Meteorological Press, 422 pp.

Ding, Y., Y. Qian, H. Yan, K. Gao, T. Shen, M. Miao, W. Li, Y. Liu, N. Zhao, L. Yi and X. Shi, 2000: Improvement of a high-resolution regional climate model and its application to numerical simulation of prolonged heavy rainfalls in East Asia. In *Development of Operational Short-term Climate Model Series 2*. Y. Ding, (Ed.), China Meteorological Press, Beijing, 217-231.

Lau, K. M., Y. Ding, J.-T. Wang, R. Johnson, T. Keenan, R. Cifelli, J. Gerlach, O. Thiele, T. Rickenbach, S.-C. Tsay, P.-H. Lin, 2000: A report of the field operations and early results of the South China Sea Monsoon Experiment (SCSMEX). *Bull. Amer. Meteor. Soc.*, **81,** 1261–1270.

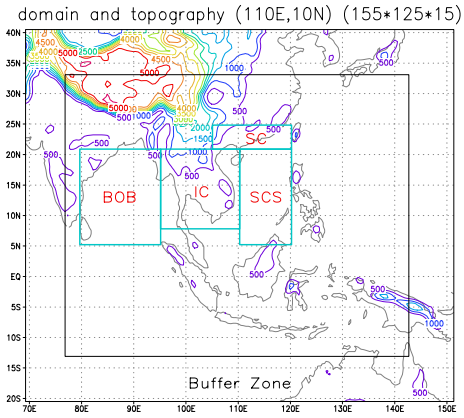

Fig. 1. The model domain and topography (contour interval: 500m).

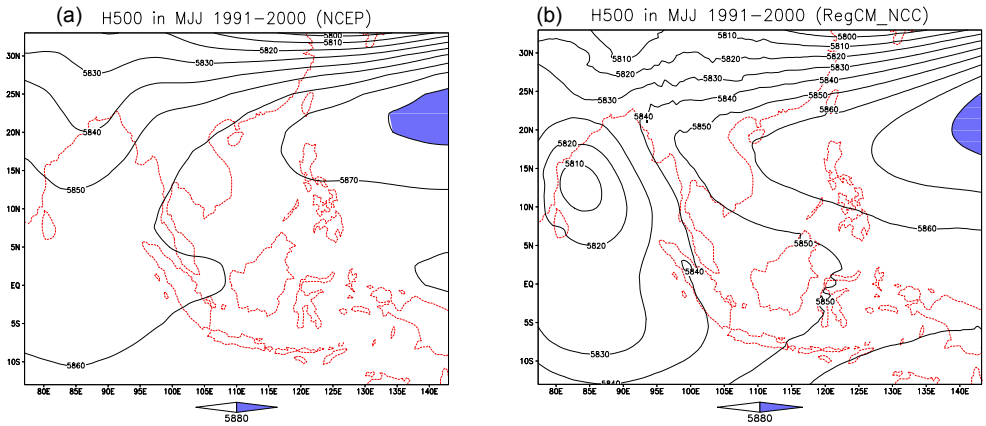

Fig. 2. 500-hPa geopotential heights averaged between May and July 1991-2000 of (a) NCEP reanalysis data and (b) simulated by RegCM. Areas with height > 5880 gpm are shaded.

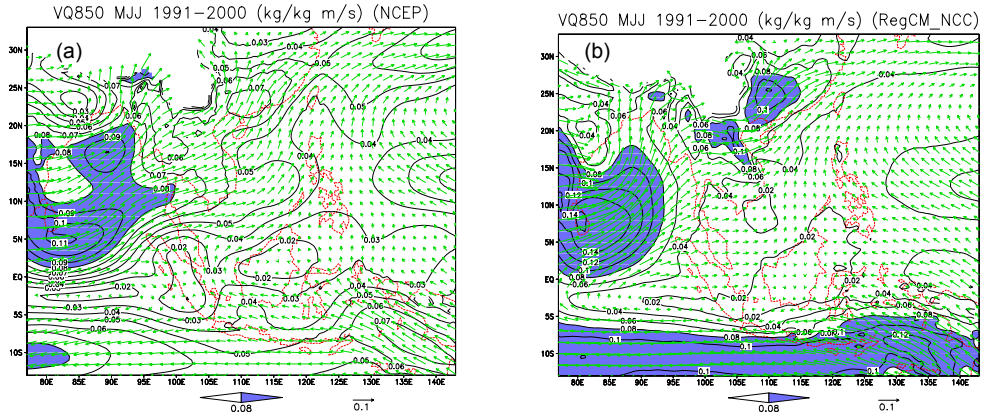

Fig. 3. As in Fig. 2 except for the 850-hPa moisture transport. Areas with moisture transport > 0.08 kg/kg m/s are shaded.

RCM's internal variability as function of domain size.

Philippe Lucas-Picher[1], Daniel Caya[2] and Sébastien Biner[2]
[1]Department of Earth and Atmospheric Sciences, UQAM, Montréal, Québec, Canada.
[2]Ouranos Consortium, Montréal, Québec, Canada.

Caya and Biner (2004) studied the Canadian RCM's (CRCM; Caya and Laprise, 1999) internal variability over an annual cycle using a small ensemble of three simulations. The CRCM domain for these simulations covers eastern North America (Fig. 1). The perturbations for each simulation in the ensemble were introduced by using different initial conditions for the atmosphere and/or the surface. The atmospheric fields used to drive the CRCM at the lateral boundary domain were taken from a GCM simulation. Annual time series of root-mean-square difference (RMSD) for various fields were chosen to quantify the CRCM internal variability. Fig. 2a presents a typical result where high values of spatial root-mean-square differences (RMSD) for the mean-sea-level pressure (mslp) are found in summer season (associated with high internal variability) and low values during the rest of the year. This means that CRCM simulations started with different initial conditions generate very similar evolution of the atmospheric fields during fall, winter and spring, but to different states during summer. A possible explanation for the summer high internal variability can be the strong summer convective activity compared to winter where the low RMSD could be associated with the less stochastic atmospheric activity. The strong winter jet stream also enhances advection through the RCM lateral boundaries and could result in a greater control on the simulations by the lateral boundary conditions (LBC) from the driving data. The opposite situation appears in summer when weaker atmospheric circulation reduces the LBC control and increases the internal variability.

Christensen et al. (2001) have shown that RCM's internal variability depends on the integration area (size and location). The present investigation aims at verifying this by making pairs of simulations with different initial conditions for various driving fields and domain sizes.

The first experiment (E1) consists in generating a pair of simulations using the same domain and driving data as Caya and Biner (2004) but with the latest version of CRCM. It can be seen by comparing Fig. 2a and 2b that the behaviour are the same in the two versions of the model. The experiment is then repeated (to generate E2) but this time with the CRCM driven by a different simulation of the Canadian GCM and over a two-year period. Fig. 2c shows a similar pattern in the RMSD for the second year but with a weaker annual cycle for the first year. A very strong peak is present at the beginning of the second year. This peak is associated with a very particular circulation making it almost unpredictable. We suspect the surface initial conditions of being responsible for the different behaviour of the first year; this aspect is currently under study. In a third experiment (E3), the driving data were taken from the NCEP reanalysis instead of a GCM simulation. Again, the analysis is performed over two years and the results appearing in Fig. 2d are very similar to what is obtained in Fig. 2c.

The next step is to investigate the influence of the domain size on the evolution of the CRCM internal variability. A fourth experiment (E4) similar to E3 was generated over a domain size nearly 2 times larger covering most of North America (Fig. 3). Large values in the RMSD time series indicate high internal variability all year long with very high values in winter season (Fig. 2e). This strong influence of the domain size might be explained by the longer residence times of the synoptic systems in the E4 domain compared to E3. These longer residence times allow for larger differences to grow in the evolution of each simulation. The generally more intense weather systems in winter added to the long residence time result in the very high RMSD values of Fig. 2e.

The results of experiment E4 suggest that as the CRCM domain gets larger, important internal variability can develop and large mismatches can also appear between the CRCM and the driving fields at the outflow boundary. An fundamental assumption in using RCM states that the large-scale atmospheric circulation in the driving data and in the RCM should remain the

same at all time. A closer look at the two simulations revealed that associated to these large RMSD are differences in the large-scale atmospheric circulation. Therefore, a last experiment (E5), identical to E4 is performed using a large-scale spectral nudging inspired from von Storch et al. (2000) to force the large-scale RCM fields toward those of the driving data. RMSD time series for E5 (Fig. 2f) showed a reduction compared to E4 but kept the higher values in winter.

These results suggest that RCM's internal variability is quite sensitive (over the first year) to the driving data used and to the size of the domain. Further investigation will be required to explain the apparent different behaviour for each year of the simulation when the CRCM is driven by the NCEP reanalysis or the outputs from the second GCM simulation.

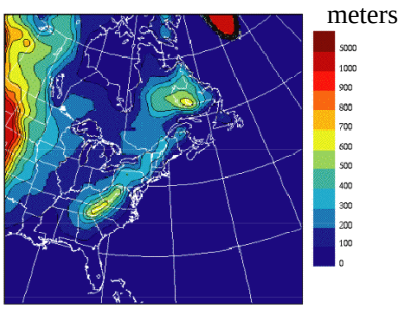

Figure 1. The CRCM domain used for Caya and Biner (2004), E1, E2 and E3. The domain contains 121X121 grid points at 45 km. RMSD time series are computed in the inner 101X101 grid points. Topographic height is shown as different shades of gray.

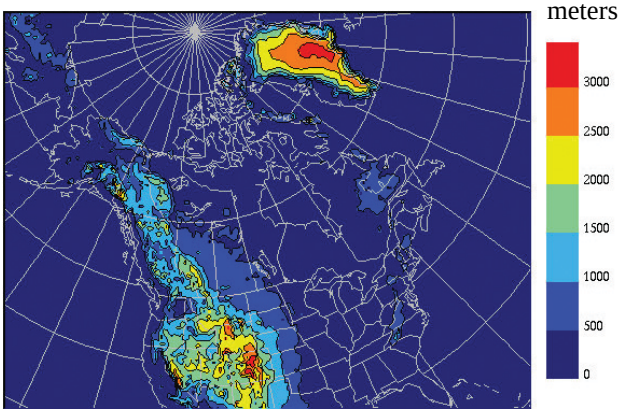

Figure 3. The CRCM domain used for E4 and E5. The domain contains 193X145 grid points at 45 km resolution. RMSD time series are computed over the inner 173X125 grid points. Topographic height is shown as different shades of gray.

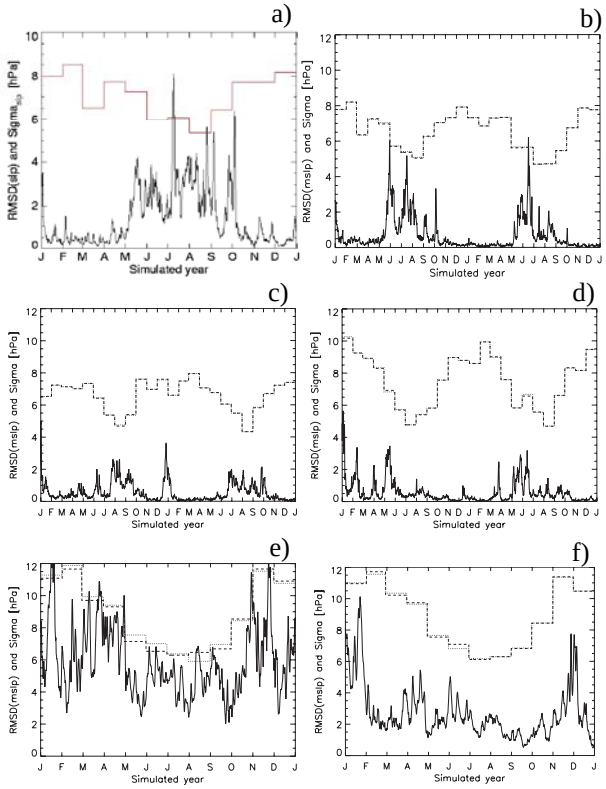

Figure 2. RMSD time series of MSLP for a) Caya and Biner (2004), b) E1, c) E2, d) E3, e) E4 and f) E5. The dotted lines show the monthly spatial standard deviation of each simulation, which are representative of the climatological value of the variability.

References

Caya, D. and R. Laprise, 1999: A semi-Lagrangian semi-implicit regional climate model: The Canadian RCM., *Mon. Wea. Rev.*, **127**(3), 341-362.

Caya, D. and S. Biner, 2004: Internal Variability of RCM Simulations over an Annual Cycle, *Clim. Dyn.*, **22**, 33-46.

Christensen, O. B., M. A. Gaertner, J. A. Prego and J. Polcher, 2001: Internal Variability of Regional Climate Models, *Clim. Dyn.*, **17**, 875-887.

von Storch, H., H. Langenberg and F. Feser, 2000: A spectral nudging technique for dynamical downscaling purposes, *Mon. Wea. Rev.*, **128**, 3664-3673.

Address any correspondence to Philippe Lucas-Picher (picher@sca.uqam.ca), Daniel Caya (caya.daniel@ouranos.ca) or Sébastien Biner (biner.sebastien@ouranos.ca).

Using Climate Models to generate Crop yield forecasts in Southeast USA

R. S Ajaya Mohan, S. Jagtap[1], T. E. LaRow, S. Cocke, J.J O'Brien, Jim Jones[1] and D. W Shin

Center for Ocean Atmospheric Prediction Studies, Florida State University, Tallahassee, FL 32306.

[1]Department of Agricultural & Biological Engineering, University of Florida, Gainesville, FL 32611.

Email: ajayan@coaps.fsu.edu

One of the major achievement in climate related studies in the last decade is the improved performance of AGCMS and CGCMS in simulating climate with respect to annual and seasonal averages. How these simulations can be used to study the local and regional impact analysis is one of the most challenging problem for the meteorologists and oceanographers. Traditionally, agricultural applications of climate forecasts have used statistical analysis of historical climate and ENSO information to arrive at climate scenarios for adaptive management. Seasonal forecasts from the state-of-the-art climate models can provide better inputs and hence can be directly linked to various application models such as crop, hydrology, ecology etc.

Since the GCMs simulations are carried out at a larger grid interval (∼200kms), downscaling the parameters for a particular station may result in inaccurate results. The regional climate models (RCMs) which is usually run at very high resolutions (∼20kms) using the boundary conditions provided by the GCM allow more accurate representation of the station data. We have used FSU Regional Spectral model (Cocke and LaRow, 2000) to generate crop yield forecasts in S.E USA. To be precise, an attempt was made to integrate outputs from the FSU regional climate Model with agricultural models to forecast maize yield in SE USA using the CERES-maize crop model.

Figure 1: : Study sites

Methodology

Seasonal integrations (March-August) of the FSU global coupled spectral model and the FSU regional spectral model has been carried out for a period of 13 years (1987-1999) using two different convection schemes. The regional model was centered over southeast U.S and run at 20km resolution, roughly resolving the county scale. Model outputs of max/min surface temperature, precipitation and shortwave radiation at the surface are used as inputs into the crop model to determine crop yields.

Comparison of regional model outputs with station observations in Florida and Georgia show that minimum surface temperatures are well simulated for the 180 day period starting from first May. The maximum temperatures show a cold bias of around 10 degrees. The model shows a wet bias in the precipitation field. Surface solar radiation shows reasonable agreement with the few stations which report that observation. The crop model is presently being run for 10 stations in south Georgia and north Florida (see Fig.1) using both the global and regional model as forcing. These stations are selected depending on the availability of crop yield data. Moreover these stations have recorded a fairly continuous record of observed surface

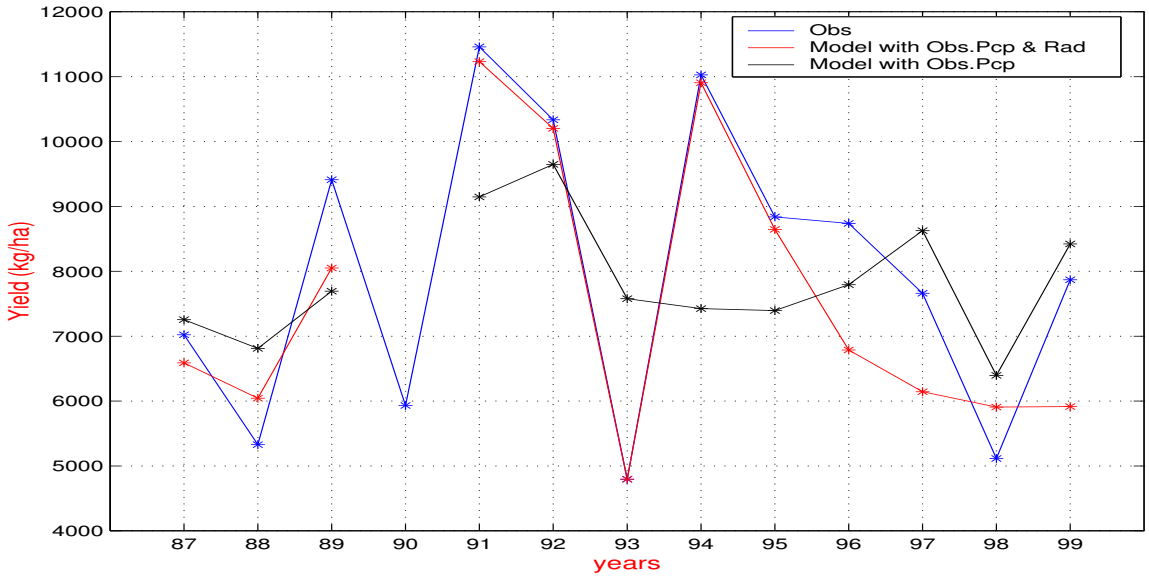

Figure 2 : Maize Yield simulated by the Crop Model using observed data and climate model data at Dublin,GA.

solar radiation. Max/Min surface temperature outputs from the model are bias corrected with respect to 13-year climatology of the observed station data. Fig.2 shows the maize yield generated by the crop model for the 13-year period with two different scenarios at a particular station in Georgia (Dublin). Blue line indicates the yield generated by the crop model using the observed station data and climatological surface radiation values were used for periods before 1995. Red line denotes the first scenario where the yield is generated using the regional model bias corrected surface temperatures and using the observed precipitation and radiation. The black line denotes the yields generated using the model bias corrected surface temperatures and radiation and using the observed precipitation. For the first case, the model performs reasonably well before 1995, but the skill is reduced after 1995. The second case performance is not good as the first case. The results indicate the need for bias correction for the precipitation field. The fact that, only by bias correcting surface temperature produces a reasonable result is promising, though a conclusive statement cannot be made at this stage of the study. Future work involves finding methods to correct the model precipitation and to see how the crop model performs in the other selected stations.

We plan on generating ten member ensembles of the regional model using different initial conditions for the entire 13-year period. These will be the used to make a probability forecast of the crop yield. We hope to correct much of the temperature and precipitation biases by using the latest version of FSUGSM which incorporates a new state-of-the-art land surface scheme and has been shown to provide better surface temperature and precipitation fields.

References

S.Cocke and T.E LaRow, Seasonal predictions using a Regional Spectral Model embedded within a Coupled Ocean-Atmosphere Model, **128**, *Mon.Wea.Rev*, 689-708, 2000.

Acknowledgment

COAPS receives its base support from the Applied Research Center, funded by NOAA Office of Global Programs awarded to Dr. James J. O'Brien.

Analysis of time lags between variations of temperature and greenhouse gases atmospheric content at Milankovitch periods from paleoreconstructions

Mokhov I.I., Bezverkhny V.A., Karpenko A.A.

A.M. Obukhov Institute of Atmospheric Physics RAS
3 Pyzhevsky, 119017 Moscow, Russia
mokhov@ifaran.ru

Analysis of time lags between temperature regime and content of atmospheric greenhouse gases from the Antarctic ice core at the Vostok station during last 420,000 years (Petit et al., 1999; Kotlyakov and Lorius, 2000) is performed (Mokhov et al., 2002; Mokhov et al., 2004). Time series of the temperature variations (T), carbon dioxide (C) and methane (M) content are studied with the use of correlation analysis (CA), cross spectral analysis (CSA) and cross wavelet analysis (CWA). Estimates of temperature variations are based on the deuterium content variations from ice core analysis (Petit et al., 1999).

The CA results show the best correlation with delay of C and M variations relative to T variations for the last 420,000 years as a whole. Similar delays are obtained for different 100,000 years sub-periods except sub-period 300,000-400,000 years B.P. (The change in the phase sign of relative variations of temperature and greenhouse gases content can be related with quality and time resolution of the data.)

The CSA results also show a general delay of C and M variations relative to T changes at Milankovitch periods (from about 20,000 years to about 100,000 years) for the last 420,000 years as a whole. Remarkable change of the sign in phase lag between T and M variations is found at periods about 20,000 years (with delay of T changes relative to M changes). It was noted both for the total 420,000 years period and for two sub-periods – for last 200,000 years and for 200,000-400,000 years B.P. (Some changes of the sign in phase lag between T and C variations at Milankovitch periods are slightly exhibited for sub-period 200,000-400,000 years B.P. without changes of the phase lag sign for the last 200,000 years.)

The CWA results display a general delay of C and M variations relative to T variations at Milankovitch time scales with differences for some sub-intervals and for selected modes (Fig.1). In particular, there is a general delay of C and M variations relative T variations for the 100,000 years mode except the last 100,000 years with phase lag of the opposite sign. The delay of T variations relative to M variations is noted also for other Milankovitch modes (with 19, 23 and 41 kyrs periods).

This work was partly supported by the Russian Foundation for Basic Research and the Russian Program for Supporting the Leading Scientific Schools.

Figure 1. Local phase lags between T and C variations from CWA: negative (blue colour) – with delay of C relative to T, positive (red colour) – with delay of T relative C (time resolution 500 years).

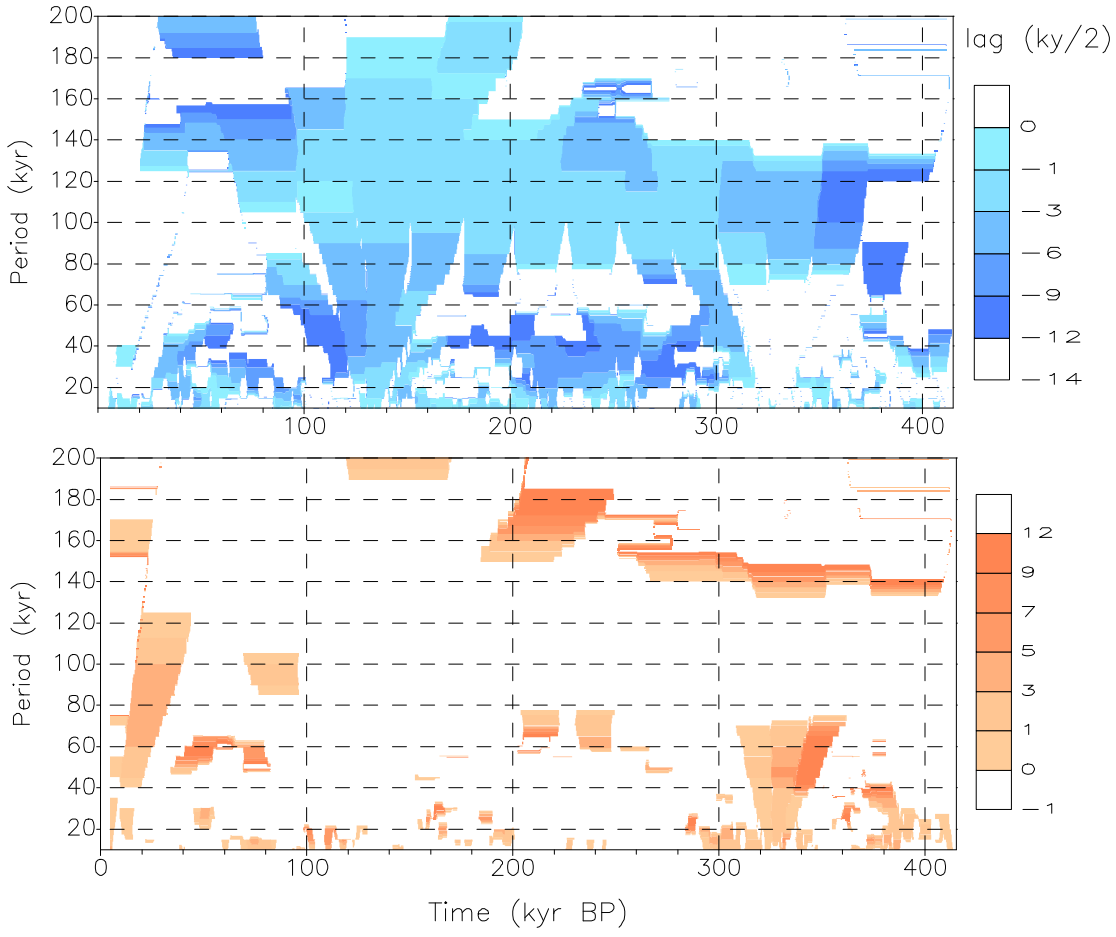

References

Kotlyakov, V.M., and C. Lorius, 2000: Four climate cycles according to the ice core data from deep drilling at the Vostok Station in Antarctica. *Izvestiya, Ser. Geograph.*, **1**, 7-19. (in Russian)

Mokhov, I.I., V.A. Bezverkhny, and A.A. Karpenko, 2002: Evolution of climatic characteristics and atmospheric components at Milankovitch scales from Vostok ice core *Research Activities in Atmospheric and Oceanic Modelling, ed. by H. Ritchie*, WMO/TD-No.1105, 2.17-2.18.

Mokhov, I.I., V.A. Bezverkhny, and A.A. Karpenko A.A., 2003: Milankovitch cycles and evolution of climatic characteristics and atmospheric components by ice core data from Antarctic Vostok station. *Data of glaciological studies*, **95**, 1-8. (in Russian)

Petit, J.R., J. Jouzel, D. Raynaud et al., 1999: Climate and atmospheric history of the past 420000 years from the Vostok ice core, Antarctica. *Nature*, **399**, 429-436.

CLIMATE EXTREMES AND NET PRIMARY PRODUCION IN EASTERN EUROPE: CHANGES IN XIX-XXI CENTURIES FROM MODEL SIMULATIONS

I.I. Mokhov (1), J.-L. Dufresne (2), H. Le Treut (2), V.A. Tikhonov (1)

(1) A.M. Obukhov Institute of Atmospheric Physics RAS, Moscow, Russia
(2) Laboratoire Meteorologie Dynamique du CNRS, Paris, France

Regional anthropogenic changes of climate extremes from simulations of a coupled atmosphere-ocean general circulation model IPSL-CM2 with a carbon cycle (Friedlingstein et al., 2001; Dufresne et al., 2002) for the 1860-2100 period are analyzed (Mokhov et al., 2002). In particular, relationships of net primary production (NPP) and drought and extreme wet conditions during spring-summer seasons are studied. Model simulations are based on anthropogenic scenario with carbon dioxide emissions due to fossil and land use from observations up to 1990 and the IPCC SRES98-A2 emission scenario from 1990 to 2100.

Model results were tested in comparison with observations from the end of the XIX century up to the end of the XX century (Meshcherskaya and Blazhevich, 1997) for Eurasian regions in the middle latitudes (Mokhov et al., 2002). For instance, model simulations reproduce quite well the decrease of precipitation anomalies with the increase of temperature anomalies during the most important period for crop development (May-July) in the Eastern European region (EER).

Different indices are used to characterize anomalously warm and dry (or cold and wet) conditions (Meshcherskaya and Blazhevich, 1997; Mokhov et al., 2002). In particular, the drought index D can be defined by the negative precipitation (normalized on the long-term mean value of precipitation) and positive surface air temperature anomalies larger than some critical values (20% for precipitation and 1K for temperature, for instance). The index W of the wet regimes can be defined by the opposite sign anomalies. The D and W values characterize the portions of total area under corresponding conditions. Two additional indices can be used: D-W and S determined by the difference of normalized temperature and precipitation anomalies (normalized on respective standard deviations).

Model results display for EER during May-July, in particular, that the increase of temperature in the XXI century relative to the XX century is accompanied in both regions by the decrease of precipitation and wet regime index and by the increase of drought indices. Simulations show the interannual variability decrease in the XXI for precipitation in EER. Drought indices display the general variability increase, while wet conditions index shows the interannual variability decrease.

Simulations show for EER significant decrease of NPP in May-July with the increase of drought index D in the XX century. No statistically significant correlation is found between NPP and D during vegetation season in EER from simulations for the XXI century. It can be interpreted as a decrease of meteorological droughts influence on NPP in EER due to the increase of the carbon dioxide atmospheric concentration in the XXI century (fertilization effect). Figure 1 shows the coefficients of correlation of NPP with precipitation (a) and with soil water content (b) for different 60-years running periods for EER from model simulations. According to Fig.1 the weakening of relationship of NPP with precipitation is accompanied by a general strengthening of NPP relationship with soil water content for EER in May-July. It is related with the change of relative contribution to NPP variations of meteorological and soil droughts.

This work was supported by the CNRS/RAS Joint Agreement Program, Russian Foundation for Basic Research and Russian Program for Supporting the Leading Scientific Schools.

References

Dufresne, J.-L., P. Friedlingstein, M. Berthelot, L. Bopp, P. Ciais, L. Fairhead, H. Le Treut, and P. Monfray, 2002: On the magnitude of positive feedback between future climate change and the carbon cycle. *Geophys. Res. Lett*, **29,** 1405, doi:10.1029/2001GL013777.

Friedlingstein P., L. Bopp, P. Ciais, J.-L Dufresne, L. Fairhead, H. LeTreut, P. Monfray, and J. Orr, 2001: Positive feedback between future climate change and the carbon cycle. *Geophys. Res. Lett.*, **28**, 1543-1546.

Meshcherskaya A.V., and V.G. Blazhevich, 1997: The drought and excessive moisture indices in a historical perspective in the principal grain-producing regions of the Former Soviet Union. *J. Climate*, **10,** 2670-2682.

Mokhov, I.I., J.-L. Dufresne, V.Ch. Khon, H. Le Treut, and V.A. Tikhonov, 2002: Regional regimes with drought and extreme wet conditions: Possible changes in XXI century from IPSL-CM2 simulations. *Research Activities in Atmospheric and Oceanic Modelling, H. Ritchie (ed.)*, WMO/TD-No.1105, 07.31-07.32.

Figure 1. Coefficients of correlation of NPP in EER with precipitation (a) and with soil water content in May-July for different 60-years running periods.

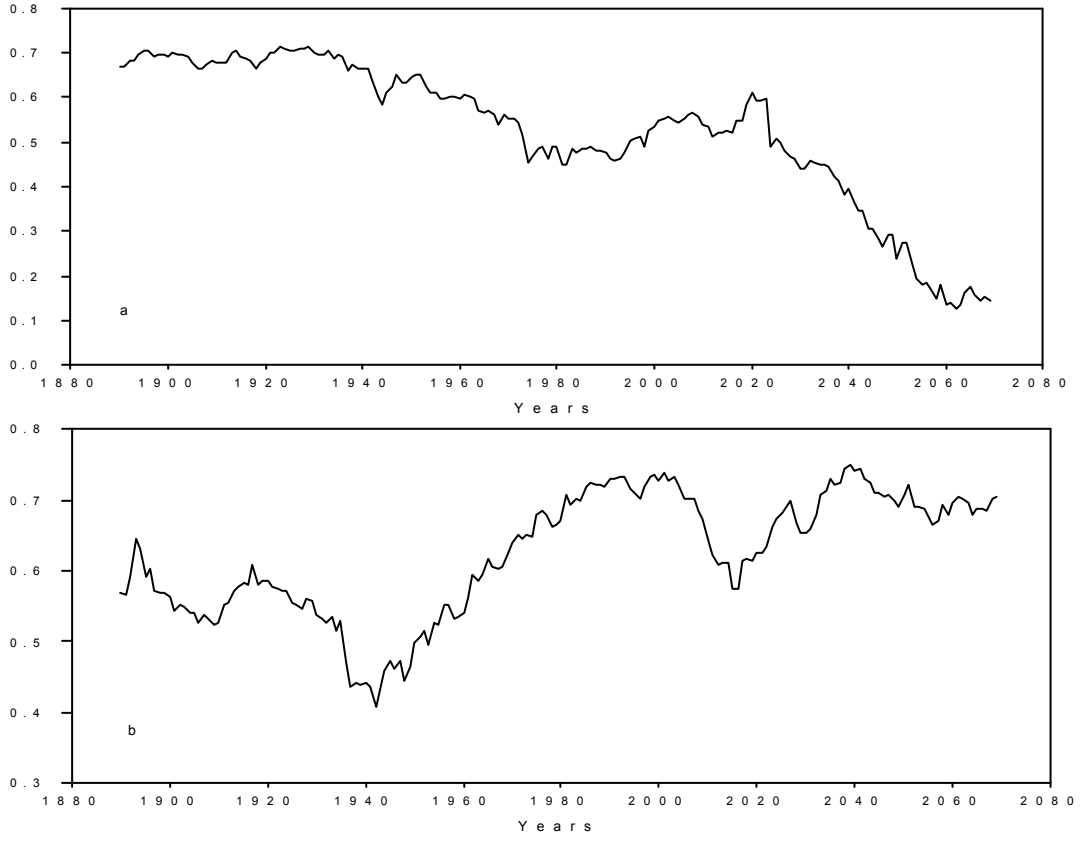

Atmospheric Centers of Action in Northern Hemisphere from Observations and Simulations: Interannual Variability and Long-Term Tendencies of Change

I.I. Mokhov, V.Ch. Khon
A.M. Obukhov Institute of Atmospheric Physics RAS
3 Pyzhevsky, 119017 Moscow, Russia (mokhov@ifaran.ru).

Interannual and long-term changes of Atmospheric Centers of Action (CoAs) in the Northern Hemisphere (NH) are analyzed using different data sets based on observations (Catalogue, 1988; Jones, 1987; Kistler et al., 2001) and global climate model simulations with anthropogenic IPCC scenarios, including coupled general circulation models ECHAM4/OPYC3 (Oberhuber, 1993; Roeckner et al., 1996), HadCM3 (Collins et al., 2001) and IAP RAS climate model (CM) of intermediate complexity (Petoukhov et al., 1998; Mokhov et al., 2002). Tendencies of change of CoAs are estimated with use of temperature data from (Jones and Moberg, 2003). Special attention is paid to winter seasons with the largest temperature changes near surface.

Sensitivity of the CoAs characteristics to the change of the NH surface air temperature (T_{NH}) can be estimated by coefficients of appropriate linear regressions. Table 1 presents coefficients of regression of CoAs characteristics to the T_{NH} variations in winter for the period 1949-2000. All analyzed data show intensification of Aleutian Low and both North Atlantic CoAs during the second half of the XX century. Tendencies of change of the Siberian High intensity from different data sets are quite contradictory.

Aleutian Low and Hawaiian High display statistically significant relationship to the El-Nino/La-Nina phenomena with intensification of this relationship to the end of the XX century. Aleutian Low deepens (weakens) and shifts eastward (westward) and Hawaiian High weakens (strengthens) and shifts southward (northward) during the El-Nino (La-Nina) events. Results of wavelet analysis exhibit the intensification of the El-Nino/La-Nina related variations (with periods about 4–6 years) of Aleutian Low and Hawaiian High at the end of the XX century.

Global climate models show an ability to simulate not just mean regimes of CoAs but also their dynamics. In particular, ECHAM4/OPYC3 simulations reproduce the relationship between North Pacific CoAs and the El-Nino/La-Nina phenomena and its intensification at the end of the XX century (Fig.1). According to these simulations the strongest correlation between North Pacific CoAs and El-Nino/La-Nina phenomena is found at the end of XX century and at the beginning of XXI century. The ECHAM4/OPYC3 model shows the intensification of Aleutian and Islandic Lows while weakening of Siberian High to the end of the XXI century with respect to the end of the XX century. The IAP RAS CM also shows the intensification of Aleutian Low and weakening of Siberian High with changes larger than for the ECHAM4/OPYC3. More significant differences are obtained for Islandic Low.

Qualitative analysis of obtained results is performed with the use of relatively simple model for the CoA characteristics proposed by Mokhov and Petoukhov (2000). According to this analytical model the long-term changes of Aleutian and Islandic Lows are related to the weakening of tropospheric static stability under warming. Significant interannual variations of Aleutian Low (related to the El-Nino/La-Nina phenomena) are in agreement with the appropriate variations of zonal wind in the troposphere. The relationship of longitudinal shift between the winter pressure maximum and cold weather center in Siberia with the El-Nino phenomenon is also interpretated on the basis of this model.

This work was partly supported by the Russian Foundation for Basic Research and the Russian Program for Supporting the Leading Scientific Schools.

References

Catalogue of Atmospheric Circulation Parameters: The Northern Hemisphere, Obninsk: VNIIGMI-MTsD, 1988 451 pp. (in Russian).

Collins, M., S.F.B. Tett, and C. Cooper, 2001: The internal climate variability of HadCM3, a version of the Hadley Centre coupled model without flux adjustments. Climate Dynamics, **17**, 61-81.

Jones, P.D. and A. Moberg, 2003: Hemispheric and large-scale surface air temperature variations: An extensive revision and an update to 2001. J. Climate, **16**, 206-223. (http://www.cru.uea.ac.uk/ftpdata/tavenh2v.dat)

Jones, P.D., 1987: The early twentieth century Arctic High - fact or fiction? Climate Dynamics, **1**, 63-75. (http://www.cru.uea.ac.uk/cru/data/pressure.htm)

Kistler, R. et al., 2001: The NCEP/NCAR 50-Year Reanalysis: Monthly Means CD-ROM and Documentation. Bull. Amer. Met. Soc., **82**, 247-266. (http://www.cdc.noaa.gov/cdc/reanalysis/)

Mokhov, I.I., and V.K. Petoukhov, 2000: Atmospheric centers of action and tendencies of their change. Izvestiya, Atmos. Ocean. Phys., **36**, 292-299.

Mokhov, I.I., P.F. Demchenko, A.V. Eliseev, V.Ch. Khon and D.V. Khvorost'yanov, 2002: Estimation of global and regional climate changes during the 19th-21st centuries on the basis of the IAP RAS model with consideration for anthropogenic forcing. Izvestiya, Atmos. Ocean. Phys., **38**, 629-642.

Oberhuber, J.M., 1993: The OPYC Ocean General Circulation Model. Max-Planck-Institut fuer Meteorologie, Rep.7, 130 pp.

Petoukhov, V.K., I.I. Mokhov, A.V. Eliseev, and V.A. Semenov, 1998: The IAP RAS Global Climate Model. Dialogue-MSU, Moscow, 110 pp.

Roeckner, E., K. Arpe, L. Bengtsson, M. Christoph, M. Claussen, L. Duemenil, M. Esch, M. Giorgetta, U. Schlese, and U. Schulzweida, 1996: The atmospheric general circulation model ECHAM4: Model description and simulation of present-day climate. Max-Planck-Institut fuer Meteorologie, Rep.218, 90 pp.

Table 1. Coefficients of linear regressions of CoAs characteristics (central pressure P_C, longitude λ_C, and latitude φ_C) to the T_{NH} variations for winters during the period 1949-2000. (Values with ** and * are significant at the 95% and 90% confidence levels).

Data	Azores High	Icelandic Low	Siberian High	Aleutian Low	Hawaiian High	Canadian High
			dP_C/dT_{NH} [hPa/K]			
NCEP/NCAR (Kistler e.a., 2001)	3.4 **	-4.2	-0.1	-5.5 **	-1.3	0.5
CRU (Jones, 1987)	3.4 **	-4.4	-5.7 *	-6.0 **	-1.3	-1.7
VNIIGMI (Catalogue, 1988)	4.8 **	-5.8 *	5.3	-7.1 **	-1.0	-1.6
			$d\lambda_C/dT_{NH}$ [deg./K]			
NCEP/NCAR (Kistler e.a., 2001)	3.0	6.8	-1.5	17.1 *	4.2	-2.1
CRU (Jones, 1987)	7.0	9.0	-6.9 *	11.8	5.1 *	15.2
VNIIGMI (Catalogue, 1988)	7.7	3.3	-2.7	5.0	-1.2	-6.6
			$d\varphi_C/dT_{NH}$ [deg./K]			
NCEP/NCAR (Kistler e.a., 2001)	0.4	2.5	0.5	-0.2	-3.4 *	-2.0
CRU (Jones, 1987)	1.9	4.1	-3.3 *	-0.8	-2.7 *	-9.3
VNIIGMI (Catalogue, 1988)	1.5	2.9	-4.3 *	1.5	-2.1	0.3

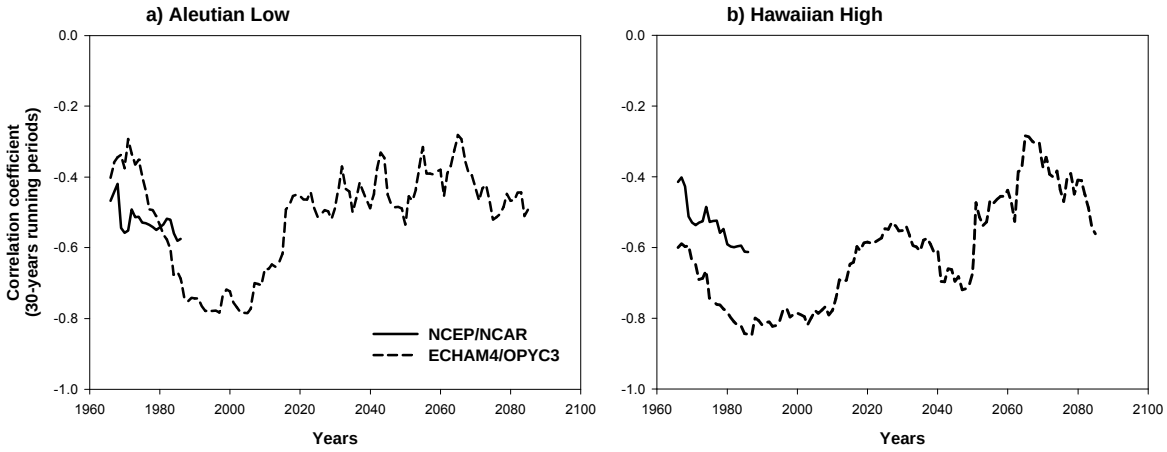

Figure 1 Coefficients of correlation between Nino3 SST and intensity of Aleutian Low (a) and Hawaiian High (b) in winter for 30-years running periods for NCEP/NCAR data and ECHAM4/OPYC3 model.

Spectral nudging in regional climate modelling: Does it induce additional gravity waves?

Hans von Storch and Frauke Feser
Institute for Coastal Research, GKSS, Germany
storch@gkss.de

The "spectral nudging" method (SN) imposes the known large-scale state on the simulation of regional climate with a RCM (von Storch et al., 2000) additional to the conventional prescription of lateral values in a "sponge zone". SN operates by adding a nudging term to the largest horizontal waves in the spectral domain. The method is a rational approach to implement the idea of state-space modelling, which combines dynamical knowledge (RCM) and empirical knowledge (the large-scale state). The method has by now been tested with several aspects with favourable results.

This method allows for superior reconstruction of space-time detailed weather than the conventional use of RCMs, with a forcing only along the lateral boundaries and in a narrow "sponge zone". SN prevents intermittent divergence in phase space (Weisse et al., 2000) and guarantees that the RCM simulates regional features consistent with a given large scale state (in the spirit of downscaling). When the method was introduced, a table was prepared, demonstrating the success of returning the same level of variability of large scales as the driving NCEP analysis, but significantly increased variability of regional scales (von Storch et al., 2000, Table 1, page 3667):

Scale/variable in 850 hPa	Unit m^2s^{-2}	NCEP reanalysis	RCM standard run	RCM with SN formulation
Zonal wind				
Large scale	10^{-2}	1.6	1.2	1.6
Small scale	10^{-6}	3.7	7.7	8.1
Meridional wind				
Large scale	10^{-2}	1.4	1.3	1.5
Small scale	10^{-6}	2.1	6.5	8.5

The table shows the spatially averaged variance of the wind in 850 hPa. This level is the lowest level at which the spectral nudging is activated. It is applied only to the two horizontal wind components.

The large-scale variability in the standard runs is slightly reduced compared to the driving NCEP re-analyses, while the SN-run reproduces or even increases the variability a bit. On the small scales (which are all not considered "large"), the variability is increased in both cases –

and it is increased in SN more than in the standard case. This last detail has caused the hypothesis that the continuously applied (small) correction would excite additionally gravity waves in the domain of the regional atmospheric model.

We have now tested this method by simply determining the time spectrum of zonal and meridional wind at a height of 10 m and of air pressure at sea level, averaged across the integration domain. Spectral densities are shown for periods less or equal 24 hours for both the standard run and the SN run. If the hypothesis would be correct, we would observe that the SN-variability of time scales of a few hours would be increased compared to the standard run. This is obviously not the case. The hypothesis may be rejected.

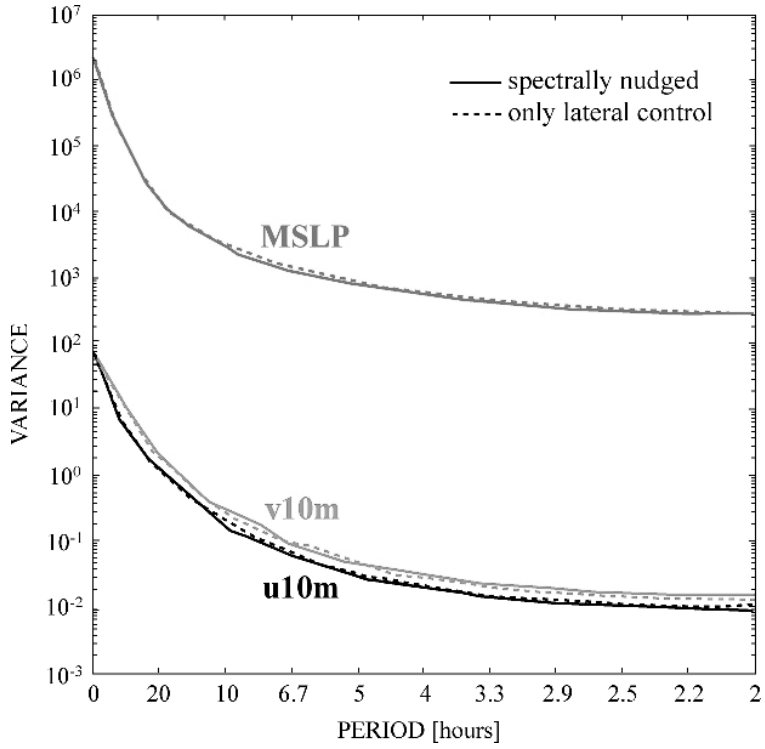

We conclude that the SN approach is not inducing additional gravity waves in a regional climate model.

von Storch, H., H. Langenberg and F. Feser, 2000: A spectral nudging technique for dynamical downscaling purposes. Mon. Wea. Rev. 128: 3664-3673

Weisse, R., H. Heyen and H. von Storch, 2000: Sensitivity of a regional atmospheric model to a sea state dependent roughness and the need of ensemble calculations. Mon. Wea. Rev. 128: 3631-3642

Using Anticyclonicity to Determine the Position of the Southern Hemisphere Westerlies: Implications for the LGM

Richard Wardle

School of Earth Sciences
The University of Melbourne
Victoria, Australia, 3010
Email: *rwardle@unimelb.edu.au*

In this work, a new perspective on the position of the Southern Hemisphere westerlies is presented. We utilize the ensemble statistics of surface high-pressure systems (anticyclones) as a dynamical determination of the westerlies. The westerlies are defined to be the westerly surface winds poleward of latitudes that correspond to the maximum anticyclone system density. A sophisticated vortex-tracking scheme (Simmonds *et al.*, 1999), applied to the results of the Melbourne University atmospheric general circulation model (MUGCM), is used to investigate the statistics of southern hemisphere anticyclones.

GCM simulation data sets for the present day (PD) and the Last Glacial Maximum (LGM) have been used in this study. Figures 1 and 2 display the characteristics of the mean system density of anticyclones for the PD and LGM simulations for DJF and JJA, respectively. The PD distributions (Figures 1a and 2a) agree well with climatology of Jones and Simmonds, (1994). Figures 1b and 2b display the same fields for the LGM, with the (LGM-PD) anomaly presented in Figures 1c and 2c (shading indicates regions of statistical significance at the 95% level). For both seasons, the anomaly patterns for each ocean sector, Australia and Southern Africa are all similar with a negative system density anomaly at approximately 30^oS and a positive anomaly near 40^oS. This anomaly pattern shows greater numbers of anticyclones at high latitudes during the LGM in each season. The ridges of anticyclonicity (the maximum system density) are plotted in Figures 1d and 2d with shading indicating longitudes of statistically significant displacement. The southern hemisphere anticyclonicity at the LGM was different to that of today in the Indian, eastern South Atlantic, much of the Pacific, and south of Australia. The position of the ridge at the LGM (solid line) is for the most part, poleward of its PD position (dashed line) during both the summer and winter seasons, which indicates a poleward displacement of the westerly surface winds. Modeled changes to the location of the ridge in South America are small.

The comparisons of the statistics of two characteristic features of the anticyclones reveal difference in the nature of atmospheric baroclinicity and the surface westerly winds. The modeled changes are also being compared to those inferred from the paleo-reconstructions.

Jones D.A., and I. Simmonds, A Climatology of Southern Hemisphere anticyclones, *Climate Dynamics*, 10, 333-348, 1994.

Simmonds, I., R.J., Murray, and R.M. Leighton, 1999: A refinement of cyclone tracking methods with data from FROST. *Aust. Meteor. Mag.*, Special Issue, 35-49.

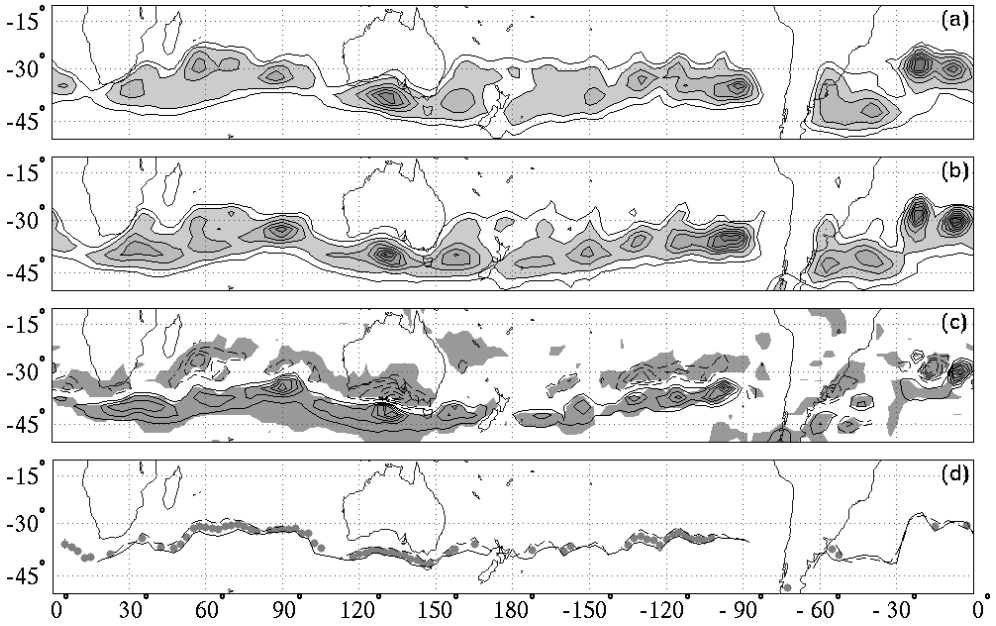

Figure 1: Anticyclone system density [the mean number per 10^3 (deg lat)^2 area] during DJF for the (a) PD, (b) LGM, and (c) the difference (LGM-PD). The contour intervals are (a)-(b) 1×10^{-3} (deg lat) $^{-2}$ and (c) 0.5×10^{-3} (deg lat)$^{-2}$. In (d), the positions of the maxima in system density for the PD (dashed) and LGM (solid) are presented with longitudes of statistical significance at the 95 % level indicated by a shaded dot.

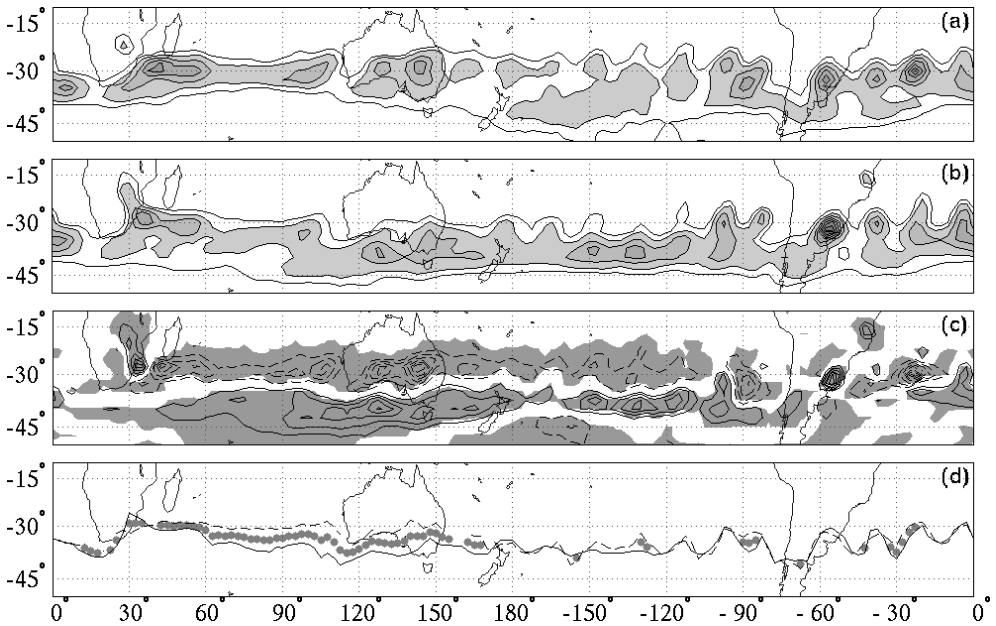

Figure 2: The same as for Figure 1, except for JJA.

Dynamical downscaling of North Sea storm surges driven by RCM simulations

Katja Woth, GKSS, Institute for Coastal Research, Geesthacht, Germany; e-mail: (woth@gkss.de)

Storm surges are one of the more direct effects of windstorms with a potential of high impact damage. The interaction between low pressure systems which determine the area of highest windspeeds and the astronomical tidal cycle leads to storm surge events the details of which depends on the geomorphological coastal structure. Storm surges and their statistics can be modelled with dynamical models (Kauker and Langenberg, 2000).

To investigate possible changes in North Sea storm surges under perturbed climate conditions, storm surge climate and extremes were derived by the barotropic storm surge model TRIM (Tidal Residual and Intertidal Mudflat) developed by Casulli and Catani: Casulli & Catani (1994) and Casulli & Stelling (1998). As forcing, a series of 30-year atmospheric regional simulations under present-day and enhanced greenhouse gas conditions were used. The effect of the expected rise in mean sea level is not taken into account. These regional simulation were prepared in the EU project (PRUDENCE (Christensen et al., 2002). The research strategy of PRUDENCE is to compare simulations of different regional models (RCMs) which are driven by the same global control and climate change simulations. These global conditions, representative for 1961-1990 and 2071-2100 were prepared by the Hadley center. Here we show results obtained by using regional model output from two models, namely HIRHAM (DMI) as well as RCA (SMHI).

The statistical analysis is carried out for the coastal cells of the modelled area, since impact damage due to human loss is expected mainly here in the coastal zone (Langenberg et al., 1999). Therefore, the model output was archived every 30 minutes at 209 coastal cells for each experiment This selection takes place from North to South of all coastal grid cells of Great Britain, then follows the continental coast from Belgium, Netherlands and Germany and ends in the North of Denmark. To identify a possible shift in the occurrence of high surge events (extremes) the resulting time series were studied with a focus on the statistical distribution, in particular on the upper tail of the distribution, i.e. the high percentiles. Since the aim of the study is the assessment of the resulting range of high surges due to the meteorological forcing simulated by different RCMs, figures 1 and 2 show a comparison between the surge along the selected 209 coastal cells forced with HIRHAM and RCA data for the winter season. Two different percentiles of storm surges, the 50- and the 99- percentiles) are shown, in each case for the CTL simulation (solid line) and the A2 SRES scenario (dashed line).

[1]

[1] **References:**

Casulli V, E. Cattani, 1994: Stability, Accuracy and Efficiency of a Semi-Implicit Method for Three-Dimensional Shallow Water Flow. Computers Math Applic 27: 99 - 112

Casulli V, G. S. Stelling, 1998: Numerical simulation of 3D quasi-hydrostatic, free-surface flows. J Hydr Eng 124: 678 - 698

Christensen, J.H., T. Carter, F. Giorgi, 2002: PRUDENCE employs new methods to assess european climate change, EOS, Vol. 83, p. 147

Kauker, F. and H. Langenberg, 2000: Two models for the climate change related development of sea levels in the North Sea. A comparison. Clim. Res. 15, 61-67

Langenberg, H., A. Pfizenmayer, H. von Storch and J. Sündermann, 1999: Storm related sea level variations along the North Sea coast: natural variability and anthropogenic change.- Cont. Shelf Res. 19: 821-842

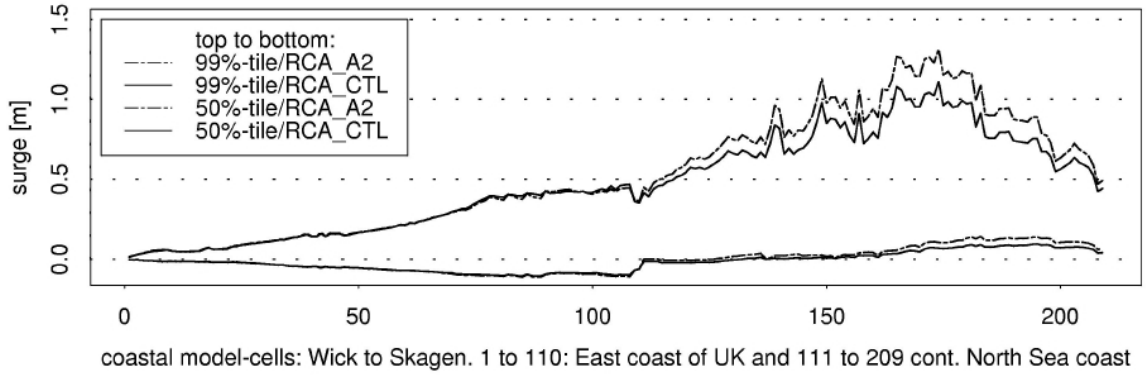

Fig.1 : Intra-annual percentiles (50 and 99) of storm surge (winter) CTL and A2 along 209 selected coastal cells. Modelled surge with meteorological forcing coming from RCA (SMHI)

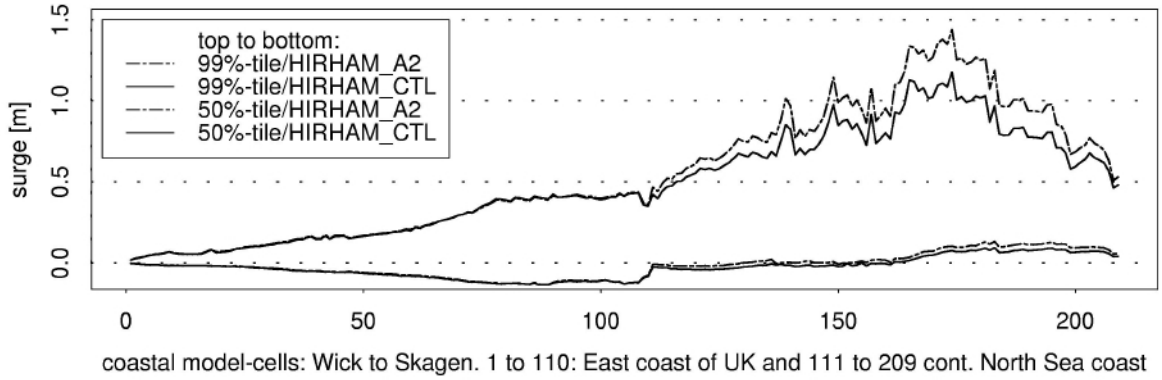

Fig.2 : Intra-annual percentiles (50 and 99) of storm surge (winter) CTL and A2 along 209 selected coastal cells. Modelled surge with meteorological forcing coming from HIRHAM (DMI)

For the control time slice, the percentiles of the modelled surge are very similar for both the HIRHAM and the RCA forcing. For the A2 SRES scenario, there is a regionally limited shift in the percentiles. An increase is noticeable only along the continental coast (right hand side of fig.1) but not along the UK coast. Furthermore, there is only a substantial increase in the high percentiles and not in the mean. The 99-percentile shows an increase of storm surge highs of up to 30 cm over several coastal cells along the Dutch coast and the German Bight. The percentiles of modelled surge with RCA forcing show a very similar pattern but are slightly weaker in the change between CTL and A2 scenario (~ up to 25 cm increase).

In respect to meet a statement about the statistical uncertainty of these estimations these first results will be extend by producing additionally storm surge model runs forced by comparable meteorological forcing data sets in the next month. Emphasis will be given to the analysis of possible changes in the occurrence of extreme storm surge events and the range of these storm surges regarding the ensemble of all available storm surge model runs.

Regional Climate Prediction using a Japan Meteorological Agency Nonhydrostatic Model with a High Resolution. Part 2: Performances of the Model with the Spectral Boundary Coupling Method.

Kazuaki, YASUNAGA[1], Teruyuki KATO[2], Yasutaka WAKAZUKI[1], Hidetaka SASAKI[2], Chiashi MUROI[2], kazuo KURIHARA[2], Yasuo SATO[2], Masanori YOSHIZAKI[2], Sachie KANADA[1], Akihiro HASHIMOTO[1]

[1]*Advanced Earth Science and Technology Organization, Tokyo*
[2]*Meteorological Research Institute / Japan Meteorological Agency, Tsukuba*

1. Introduction

We are trying to predict climate around Japan using a high-resolution nonhydrostatic model that is nested within a global climate model (GCM) when concentrations of carbon dioxide in the atmosphere increase (Kato et al. 2004). Earth Simulator, which is the fastest computer around the world, has enabled long-term prediction by a nonhydrostatic model with a horizontal grid of a few kilometers.

For the high-resolution long-term prediction, a nonhydrostatic model developed jointly by the Meteorological Research Institute and Numerical Prediction Division, Japan Meteorological Agency (Saito et al., 2001, JMA-NHM) is applied. JMA-NHM has been used for the short-term prediction (less than 1 day). Therefore, to use JMA-NHM as a regional climate model, some improvements and evaluation of model performances are necessary.

The Spectral Boundary Coupling (SBC) method, which the Meteorological Research Institute, JMA (MRI) has been developing (ref. Kida et al. 1991), is introduced into JMA-NHM for the purpose of conducting regional climate simulations. The SBC method is the technique of nesting a high-resolution limited area model in such a low-resolution global model as GCM. In practice, the SBC method is to replace the large-scale fields (the long wave part) of a fine mesh model with the corresponding large-scale fields supplied externally from a coarse mesh model. When the conventional nesting method is used, the lateral boundary of an inner fine mesh model is adjusted only to the limited area of an outer coarse mesh model in real space, and other information of the outer coarse model has no effects on the fine mesh model. On the contrary, when the SBC method is used, the connection between the two models is made in wave number space. Accordingly, with the SBC method, the discrepancies between the phases and the positions of disturbances in the two models (fine and coarse mesh models) can be small, and the long-term integration could be is conducted smoothly.

Sasaki et al. (1995) and Sasaki et al. (2000) used the objectively analyzed fields instead of the forecasts of GCM, and it was found that two limited areas models for the regional climate simulation with resolutions of 127 km and 40 km reproduced the objective analysis with a high accuracy when the SBC method was employed. The models are hydrostatic models, and the dynamical and physical frameworks of the two models are similar to those of GCM or the model used for objective analysis, and such similarity is favorable to suppress noise when the long wave part is replaced in the SBC method. On the other hand, JMA-NHM is a nonhydrostatic model with cloud microphysics, and much finer resolution is generally employed for the regional climate simulation. Therefore, it is unknown that the SBC method also works well for such a model with different dynamical and physical frameworks. In the present study, it is investigated that whether the long-term simulations by the high-resolution JMA-NHM show high performances when the SBC method is used.

*Corresponding author address: Kazuaki YASUNAGA, Meteorological Research Institute, 1-1 Nagamine, Tsukuba, Ibaraki 305-0052 Japan: e-mail: kyasunag@mri-jma.go.jp

2. Numerical Model and Experimental design

The horizontal grid size of JMA-NHM used in this study is 5 km, and the domain covers 4000 km x 3000 km. The model has 48 vertical layers, and the 6-hourly regional analyses of JMA are used instead of the forecasts of GCM. The integration starts from 20 May, 2003, and its period, including the rainy season of Japan, is 70 days. The major specifications of JMA-NHM and experimental designs are detailed by Kato et al. (2004).

3. Results and Conclusions

Figure 1 shows the analyzed and predicted sea level pressure fields after the integration of 10 days. When the SBC method is employed (Fig. 1b), the value of sea level pressure at the center of a depression (988 hPa) agrees with the analysis, and the center is predicted close to the analyzed position. On the other hand, when the SBC method is not employed (Fig. 1c), the value of sea level pressure at the center (1000 hPa) is much lager than that of the analysis, and the center is predicted apart from the analyzed position.

Figure 2 represents time series of the root mean square error (RMSE) of sea level pressure for the

objectively analyzed values over the model domain. The RMSEs in the prediction with the SBC method (the red line in Fig. 2) are much smaller than those without the SBC method (the green line in Fig. 2).

The following verifications were conducted in order to examine the performances of the SBC method over Japan and five local regions of Japan. Figure 3a shows correlation coefficients between observed and predicted surface temperature, and Fig. 3b shows RMSE of precipitation during the simulation period (The predictions during the first 11 days of integration are not verified in order to exclude the influence of the initial fields). When the SBC method is employed, the correlation coefficients (Fig. 3a) and the RMSE of precipitation (Fig. 3b) are lager and smaller over all regions than those when the SBC method is not employed, respectively.

As verified above, all results of JMA-NHM are improved, by using the SBC method. Therefore, it is concluded that the SBC method could work well even for a nonhydrostatic model with the high-resolution.

Acknowledgements

This study is conducted by the fund of Research Revolution 2002, and the numerical calculations are made by NEC SX-6 on Earth Simulator.

References

[1] Kato, T., K. Yasunaga, C. Muroi, M. Yoshizaki, S. Kanada, A. Hashimoto, Y. Wakazuki, H. Eito, S. Hayashi, and H. Sasaki, 2004: Regional Climate Prediction by using a Japan Meteorological Agency Nonhydrostatic Model with a High Resolution. Part 1: Outline/Purpose of a High-Resolution Long-Term Prediction. *CAS/JSC WGNE Research Activities in Atmospheric and Oceanic Modeling, submitted.*

[2] Saito, K., T. Kato, H. Eito and C. Muroi, 2001: Documentation of the Meteorological Research Institute / Numerical Prediction Division Unified Nonhydrostatic Model. *Tech. Rep.of MRI*, **42**, p133.

[3] Kida, H., T. Koide, H. Sasaki, and M. Chiba, 1991: A new approach to coupling a limited area model with a GCM for regional climate simulations, *J. Meteor. Soc. Japan, **69**, 723-728*

[4] Sasaki, H., Y. Sato, K. Adachi, and H. Kida, 1995: The performance of long-term integration of a limited area model with the spectral boundary coupling method. *J. Meteor. Soc. Japan, **73**, 165-181*

[5] Sasaki, H., Y. Sato, K. Adachi, and H. Kida, 2000: Performance and Evaluation of the MRI Regional Climate Model with the Spectral Boundary Coupling Method. *J. Meteor. Soc. Japan, **78**, 477-489*

(a)

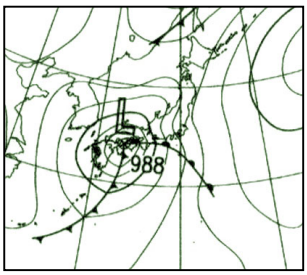

(b)

(c)

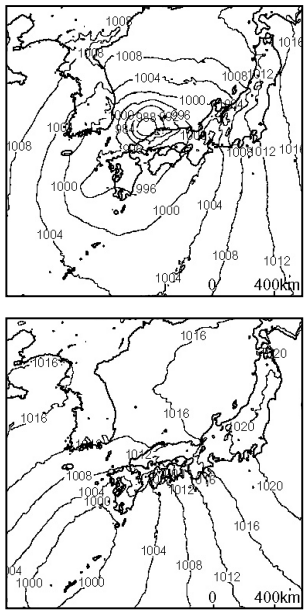

Fig. 1 (a) Analyzed sea level pressure at 09 JST on 26 May 2003, predicted sea level pressure (b) with SBC method, and (c) without SBC method.

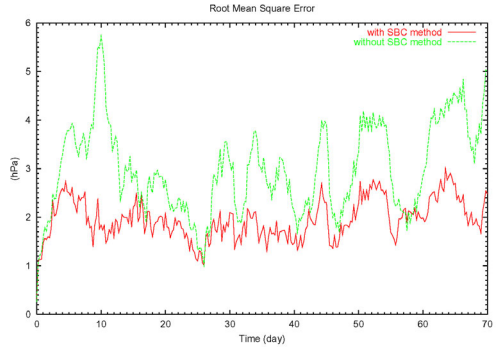

Fig. 2 Time series of the root mean square error of sea level pressure (a green line: with the SBC method, a red line: without the SBC method).

(a)

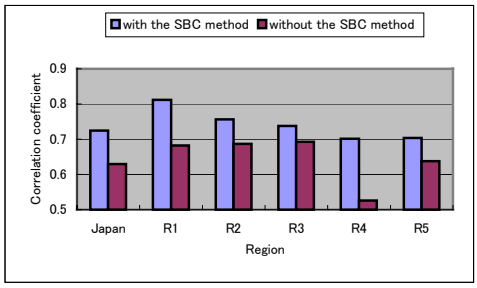

(b)

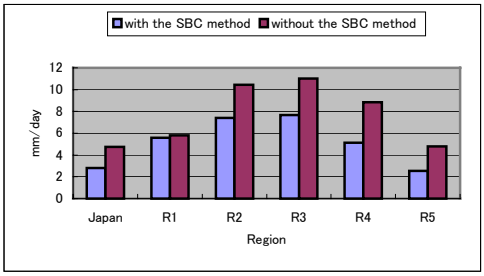

Fig. 3 (a) correlation coefficients between observed and predicted surface temperature, and (b) RMSE of the precipitation during the simulation period.